The Pennsylvania State University

The Graduate School

College of Engineering

EXPERIMENTAL EVALUATION OF FLUIDIC FLEXIBLE MATRIX COMPOSITE ACTUATORS

A Thesis in

Aerospace Engineering

by

Benjamin Wimmer

Submitted in Partial Fulfillment
of the Requirements
for the Degree of

Master of Science

December 2012

The thesis of Benjamin Wimmer was reviewed and approved* by the following:

Charles E. Bakis
Distinguished Professor of Engineering Science and Mechanics
Thesis Co-Advisor

Dennis K. McLaughlin
Professor of Aerospace Engineering
Thesis Co-Advisor

George A. Lesieutre
Professor and Head of the Department of Aerospace Engineering

*Signatures are on file in the Graduate School

ABSTRACT

A unique quality of composites made with a stiff reinforcement fiber and soft matrix material is that they are able to deform in complicated ways when stresses are applied due to highly directional stiffness properties. When this ability is employed in a tubular structure filled with fluid, interesting shape and stiffness changes can occur as a function of the pressure applied to the fluid. These tubes, called fluidic flexible matrix composites (F^2MCs), are a new type of adaptive material. Until recently, most research and experimentation on F^2MCs has been with simple thin walled filament wound tubes. There is currently a push to develop different variations of this concept suitable for a variety of applications. For example, some applications call for embedding the F^2MC tubes into stiffer materials and others might need smaller and lighter tubes than those that can be made by filament winding. The objectives of this investigation are to investigate the performance filament wound F^2MCs embedded into stiffer media and the performance of small-diameter braided F^2MCs. Three main ways were employed to evaluate the performance of F^2MC's: free axial strain versus pressure; axial force versus pressure in the blocked condition (no axial strain); and the axial modulus of elasticity without any internal fluid. Some key results obtained from these test include large underperformances of F^2MC actuators versus predictions, especially in several of the blocked force tests. As can be expected, large drops in performance accrued when F^2MCs were placed into a stiff medium. It was also found that small diameter braided F^2MCs could be made and used as actuators. It is suggested that more research into the three dimensional properties and states of deformation of the various composites might improve correspondence between theory and experiments. Factors such as interlaminar shear deformation, viscoelasticity, and end effects due to the grip fittings should be further explored, as well.

TABLE OF CONTENTS

LIST OF FIGURES

LIST OF TABLES

ACKNOWLEDGEMENTS

I would like to express my deep gratitude to Professor Dr. Charles E. Bakis, my research advisor, for his patient guidance, enthusiastic encouragement and useful critiques of this research work. I would also like to thank him for his advice and assistance in keeping my progress on schedule. I would also like to thank Mr. Bin Zhu for all of his help with running experiments, fabricating test specimens, and all the calculations he did to predict the responses of specimens I was testing. I am also thankful to Dr. Chris Rahn for advice and brainstorming assistance. Advice given by Dr. Dennis McLaughlin and Dr. Thomas Juska has been a great help to me in conducting my research.

This research was sponsored by the National Science Foundation (NSF) Emerging Frontiers in Research and Innovation (EFRI) Program under Grant Number 0937323. Any opinions, findings and conclusions or recommendations expressed in this material are those of the author and do not necessarily reflect the views of NSF.

I would also like to thank the staff at New England Catheter Corp. for their assistance in working with me to develop custom made tubes for me to test. I am particularly thanks full for assistance given to me by Mr. Simon Miller, Mr. Todd Henry, Mr. Pat Mangiagli and Mr. Ardell Hosterman for all of their assistance and guidance with lab equipment and software. Finally I would like to thank my family and friends for supporting me and helping get through tough and stressful times.

Chapter 1

INTRODUCTION

Background

Ever since the development of composites there has been a lot of research into the many possibilities they offer. With seemingly endless possibilities to tailor structures to one's needs, composites created many new possibilities for creating innovative structures. Interesting and unique capabilities have been recently seen with filament wound composites comprising stiff fibers such as carbon embedded in a highly flexible, elastomeric matrix like polyurethane. It has been found by that such tubes are filled with a fluid and, by using a valve to control the flow of fluid into our out of the tube, have been shown to have a variable axial stiffness [1] The fluid with a high bulk modulus resists volume change that would normally occur with an open valve. So, by closing the valve, the tube becomes much stiffer than in the open valve case. By varying the fiber angle and matrix material of these tubes there are nearly endless stiffness ratios that can be obtained. Similarly, by varying the internal pressure, the tube behaves like an actuator. Tubes with fiber angle less than ±55 degrees relative to the longitudinal axis will axially contract while tubes with fiber angles greater than ±55 deg. will axially extend. It has been shown that large strain and force can be achieved by such tubes [2-4]. These tubes have come to be known as fluidic flexible matrix composites or F^2MC.

With the ability to actuate and have variable stiffness, F^2MC's are suited well for adaptive structures. Fluidic flexible matric composites (F^2MC) actuators have been shown to give a high mechanical advantage [2-4], making them an effective adaptive structure that can

rapidly change shape with minimal energy usage. The need for structures like these extends to aircraft [5], watercraft [6], wind turbines [7], and even buildings [8].

The performance potential of various F^2MC tubes have been compared in terms of a three basic characteristics:

1. Free strain per unit pressure change. This is the change in axial strain per unit internal pressure change when no axial force is applied to the tube;
2. Blocked force per unit pressure change. This is the change axial force per unit internal pressure change when there is no change in axial strain;
3. Axial modulus. This is the change in axial stress (axial force divided by net wall area of the hollow tube) divided by the change in axial strain, when no internal pressure change occurs.

To-date, investigations of F^2MCs have been done using single layer filament wound tubes, where all the fibers in the tube are wound at a $\pm\theta$ angles, where the angle is measured relative to the longitudinal axis of the tube. In applications such as adaptive skins, it may be necessary to embed arrays of F^2MC tubes into some other structural material. However, until now, there has not been any systematic research on the performance of F^2MC tubes embedded inside a structural material. Also, F^2MC tubes demonstrated to-date have had diameters measured in centimeters. Since many applications may require smaller tubes, research is needed on the performance of F^2MC tubes of sub-centimeter diameters.

The objectives of this investigation are as follows:

1. Evaluate the performance of filament wound F^2MC tubes embedded inside of a relatively stiff composite material. This topic is covered in Chapter 2.
2. Evaluate the performance of a filament wound F^2MC tube embedded in an isotropic polymer. This topic is covered in Chapter 3.

3. Evaluate the performance of miniature braided F^2MC tubes. This topic is covered in Chapter 4.

Chapter 2

Large Filament Wound F^2MC Tubes Embedded in a Composite Medium

Introduction

Tubes demonstrated in previous investigations consisted of thin FMC outer walls, sometimes with a thin, soft, elastomeric inner wall for blowout prevention. The objective of the work described in this chapter is to evaluate the performance potential of "large" F^2MC tubes embedded inside a relatively stiff composite medium. Based on an analysis reported in [9], it was determined that superior performance could be realized by using a thick-walled filament wound FMC inner tube as the actuator and a second thick-walled filament wound FMC outer tube as the composite structural medium. The thick walls, together with the low radial modulus of elasticity of filament wound FMC tubes, allows the inner actuator region to expand and contract circumferentially with minimal constraint from the outer structural region. At the same time, it is hypothesized that the inner actuator can still significantly affect the overall stiffness and shape of the entire dual-tube structure by the effective transmission of axial forces between the tubes.

Experimentation

Materials

Constituents

Hexcel HexTow AS4D-12K carbon fiber with an elastic modulus of 245 GPa [10] was used to wind the F^2MC actuator and the surrounding medium. For the bi-layer tubes representing an actuator inside of another medium, two different flexible polyurethane resins from Smooth-On were selected for the inner and outer layer matrix materials. The inner layer contains Reoflex 20 with a 100% modulus of 0.186 MPa while the outer layer contains Reoflex 60 with a 100% modulus of 1.77 MPa [11]. Fiber selection was based on modulus, while the matrix selection was not only based on modulus as suggested by previous analysis [9] but also on acceptable mix viscosity and pot life. The softer matrix used for the inner (actuator) layer is intended to soften the radial coupling between that layer and the stiffer outer layer, thus improving actuator performance.

Manufacturing method

The tubes were wet-wound on a 4-axis, computer controlled filament winder with electronic tow tensioning. Fiber was wound onto a steel mandrel. The mandrel was prepared by first polishing the surface with a Scotch Brite pad and then cleaning with acetone and a cloth until the cloth remained clean. After the mandrel was cleaned, a silicone release spray was applied to the surface of the mandrel and the mandrel was then left in ambient laboratory air to dry. The release-sprayed mandrel can be placed into an oven to help speed up the drying process. Once the mandrel dried, one or two more coatings should be applied following the same process as

described above. Once the final release coat was dried, the mandrel was placed into the filament winder. The tow was then run through the resin bath. A precision orifice with an inside diameter of 0.965 mm was used to meter the correct amount of resin in the tow after the tow passed over the wet bars of the bath. One tow was wound at a time, with a tension of 4.5 N. Since there was no resin drip-off due to the high viscosity of the liquid polyurethane resins, it is assumed that the final fiber volume content can be calculated from orifice cross-sectional area, or 58%. Once the tow was threaded through the resin bath and placed on the mandrel, the polyurethane matrix material was mixed and put into the resin bath. With resin now in the bath, the tow was pulled through until wetted fiber could be tied onto the mandrel. Next, a machine control program was set up to wind the tube based on the desired fiber angle and the diameter of the mandrel. It is important to note that for each layer wound onto the mandrel the outer diameter changes and new programs must be made to have a consistent fiber angle through the thickness. Ply thickness, based on a programmed bandwidth of 2.3 mm, was estimated to be 0.5 mm. Finally after all the layers were wound, one layer of release-coated shrink tape (Hi-Shrink Tape, 25-mm wide, 0.05-mm thick, 80°C activation temperature, from Dunstone Inc., Charlotte, NC) was wrapped by hand around the tube to help consolidate the fibers and matrix. It was wound trying to keep a constant tension on the tape and overlapping half of the tape width.

Based on preliminary testing and calculations not reported here for conciseness, the effective Young's moduli, E, Poisson's ratios (ν) and shear moduli (G) of the two composites in unidirectional form are as shown in Table 2-1. The 1-direction is the fiber direction and the 2-3 plane is assumed to be a plane of transverse isotropy. These properties were used in the work by Zhu et al. in [9] to design and analyze the tubes used in the current experiments.

Table **2-1**: Unidirectional composite properties used in models of large tubes.

Lamina property	AS4/Reoflex20 (inner layer)	AS4/Reoflex60 (outer layer)
E_{11} (GPa)	115	115
E_{22} (MPa)	30	285
ν_{12}	0.33	0.33
ν_{23}	0.93	0.93
G_{12} (MPa)	$0.86E_{22}$= 25.8	$0.86E_{22}$= 245

Two single-layer specimens were made entirely of AS4/Reoflex20—one thin and one thick—for evaluation of the effects of actuator thickness and surrounding medium on actuator performance (Table 2-2). Five bi-layer specimens had 5-mm-thick inner layers of AS4/Reoflex20 as suggested in [9] to help radially decouple the actuator from the surrounding medium. The inner layer fiber angles were selected for contraction (<55°) or extension (>55°) actuation behavior. The 2.5-mm-thick, ±57° outer layer of AS4/Reoflex60 provided a structurally stiff surrounding medium with negligible extension or contraction under internal pressurization. The radial, hoop, and axial Young's moduli of the outer layer are 0.95, 2.8, and 0.51 GPa, respectively, according to an analysis by Mr. Bin Zhu. In the bi-layer specimens, the inner F^2MC actuator region represents roughly 74% of the cross section of the specimen, which is the theoretical maximum if the FMC actuators were to be tight-packed in a square array in a "smart skin." The inner, intermediate, and outer radii (a_1, a_2, and a_3, respectively), number of winding layers per material layer, and fiber angles relative to the axial direction are given in Table 2-2. The finished tubes had lengths of 270 mm. Threaded pipe fittings were bonded into the ends of the specimens seen in Figure **2-1** using a two part methacrylate adhesive, Devcon Plastic Welder (ITW Devcon, Danvers MA). The threads are a ¾ NPT and the length of embedment into the tube

is approximately 38 mm. The outside of the specimen was squeezed onto the fittings with T-bolt hose and tube clamps (McMaster-Carr, Aurora, OH.)

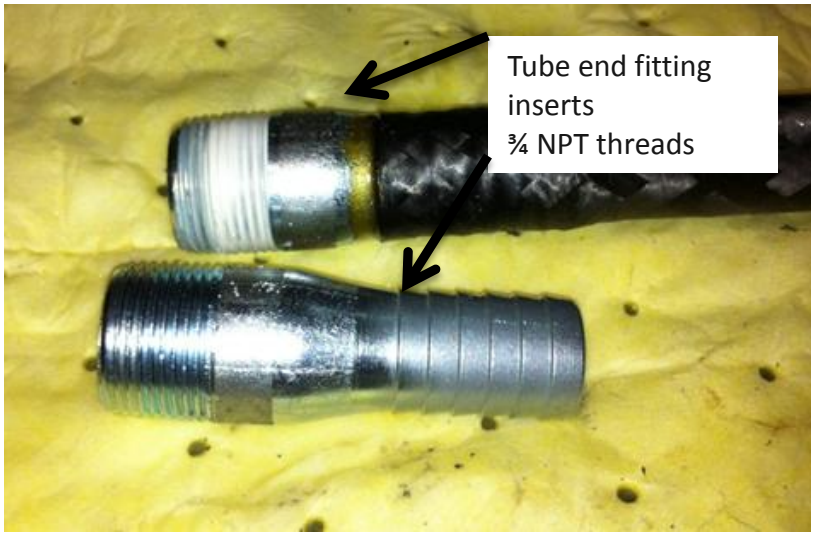

Figure **2-1**: Threaded tube fittings.

Table **2-2**: Specimen characteristics for large tubes.

Tube	**Layer Radii**			**Inner Layer**		**Outer Layer**	
	a_1 (mm)	a_2 (mm)	a_3 (mm)	# Wind Layers	Angle (±°)	# Wind Layers	Angle (±°)
35° Thin	10	N/A	11.1	2	35	N/A	N/A
35° Thick	10	N/A	15	8	35	N/A	N/A
12.5° Bi-layer	10	15	17.5	8	12.5	4	57
22.5° Bi-layer	10	15	17.5	8	22.5	4	57
38.3° Bi-layer	10	15	17.5	8	38.3	4	57
52.5° Bi-layer	10	15	17.5	8	52.5	4	57
62.5° Bi-layer	10	15	17.5	8	62.5	4	57

Tests

Three types of tests were carried out to characterize the mechanical behavior of the specimens: free strain, blocked force, and axial modulus. The testing apparatuses seen in Figure **2-2** included a load frame into which the specimens were pinned through the end fittings, two 25-mm gage length clip-on extensometers positioned at the mid-length position of the specimens on opposite sides for measuring average axial strain, a hand-pump, and mechanical and electronic pressure transducers. The servo-hydraulic load frame has a 22 kN load cell and an actuator with a 150-mm stroke. The load and stroke ranges used for the investigation were 445 N/V and 7.6 mm/V, respectively. The hydraulic hand-pump was conservatively limited to 4 MPa to prevent leaks at the various fitting junctions. The electronic pressure transducer was calibrated to about 1.6 MPa/V.

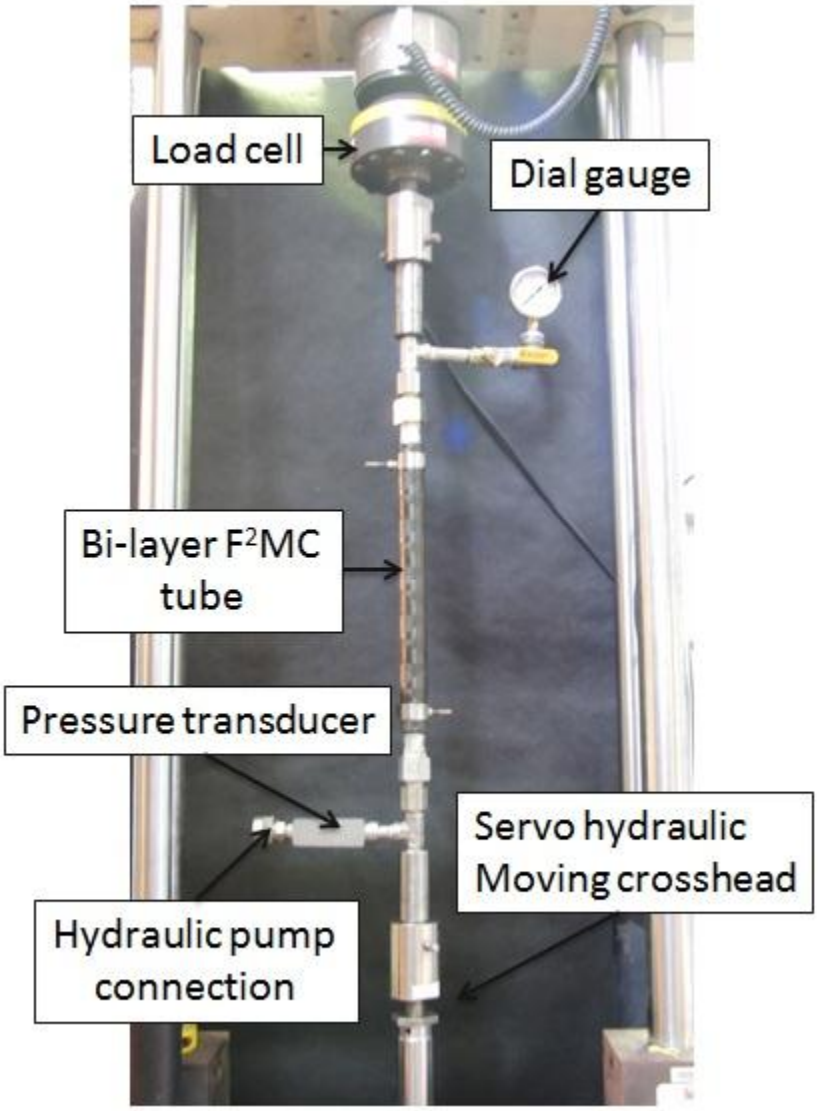

Figure **2-2:** Test apparatus for large tubes.

For the free strain tests, one end of the specimen was pinned into the load frame and the other left free to move axially. Hydraulic fluid was pumped into the specimen to a pressure of about 4 MPa for the bi-layer and thick single-layer specimens and about 1 MPa for the thin-walled specimen. A basic representation of the free strain case can be seen in Figure **2-3**. The extensometer strains were recorded as pressure was varied manually. Four pressure cycles were

performed to establish a “steady state” response. Due to some softening of the FMC material (e.g., the Mullins effect [12]) on the initial pressure cycle, the strain versus pressure data on the first cycle was discarded and the recorded results were confined to the second, third, and fourth cycles. For each pressurization/depressurization cycle, the axial strain versus pressure slope was found by fitting a straight line by the least-squares method to both the pressurization and depressurization halves of the cycle. The final strain versus pressure slope assigned to each tube was found by averaging the slopes from the last three pressure cycles.

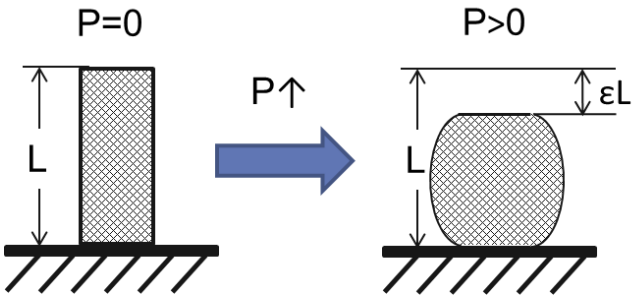

Figure **2-3**: Free strain test diagram.

For the blocked force test, both ends of the specimen were fixed by pins to the load train. The servo-hydraulic test frame was set to displacement control to keep a fixed overall distance between the pins. A small tensile preload of 100 N was applied to prevent buckling in cases where the specimen increased in length with pressurization. Using the load cell of the load frame, axial force was measured as the internal pressure increased to 4 MPa for the thick specimens and 1 MPa for the thin-walled specimen. A diagram of the blocked force test can be seen in Figure **2-4**. The force versus pressure relationship for each pressure cycle was found from the slope of the straight line fit by least squares to the entire pressurization-depressurization cycle. As with the free strain test, an average of the second, third, and fourth slopes was calculated for each specimen.

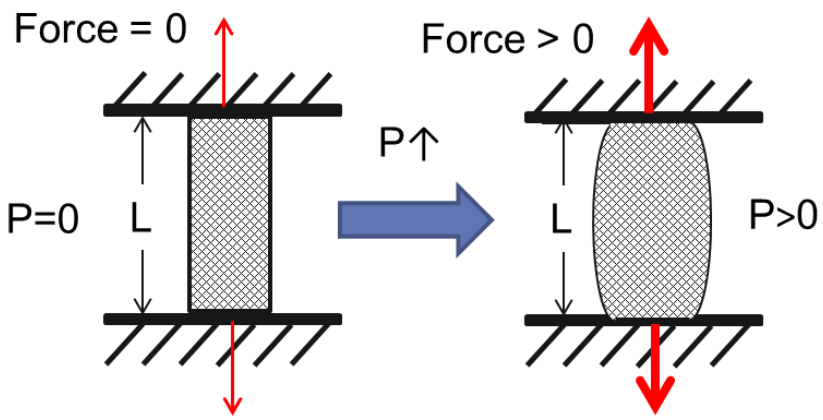

Figure **2-4**: Blocked force test diagram.

For the axial modulus test, empty specimens were pinned at both ends to the load frame. Tensile forces of up to 100 N were applied while longitudinal strains were recorded with the two extensometers mentioned earlier. Axial modulus of elasticity, defined as the applied stress divided by the average axial strain, was computed based on only the load-up cycle (not the unloading cycle as well). Stress in these experiments is defined as the force divided by the net cross-sectional area of the wall of the hollow specimen. The crosshead was actuated using displacement control at a rate of about 0.025 mm/sec.

Experimental results were compared to a closed-form and finite element predictions of specimen performance generated by Mr. Bin Zhu. The elasticity solution is for a pair of concentric, perfectly bonded, infinitely long, layered orthotropic tubes under internal pressurization and axial force. The finite element analysis (FEA) is for a similar pair of tubes of length equal to the actual length of the specimens tested in this investigation, with rigid end fittings simulating the experimental end fittings. Therefore, the FEA solution was expected to capture end effects that are not included in the analytical solution.

Results

Free strain

Figure **2-5** and Figure **2-6** show the free strains in thin and thick 35° single-layer specimens, respectively. The thin contractor tube matches fairly well with the analytical model. It can be seen that there is a significant amount of creep due to viscoelastic effects which is present in all tubes tested in free strain. In the thick-walled tube, it is seen that the tube actually contracts about 5 times that predicted by the analytical model. Further investigation is needed to determine the reason for this discrepancy.

Free strains for the 12.5° bi-layer tube are shown in Figure **2-7**. The data are inconstantly scattered around zero strain. This tube is predicted to contract very small amounts even at high pressures. Sensitivity limits of the extensometers lead to little meaningful information in this experiment. For the 22.5° bi-layer tube shown in Figure **2-8**, there is sufficient strain to be measured, producing results that match well with the predictions of the analytical and FEA models. Nonlinear behavior and hysteresis are also evident. These are thought to be due to in-plane shear-dominated behavior and viscoelastic effects in the FMC material, respectively.

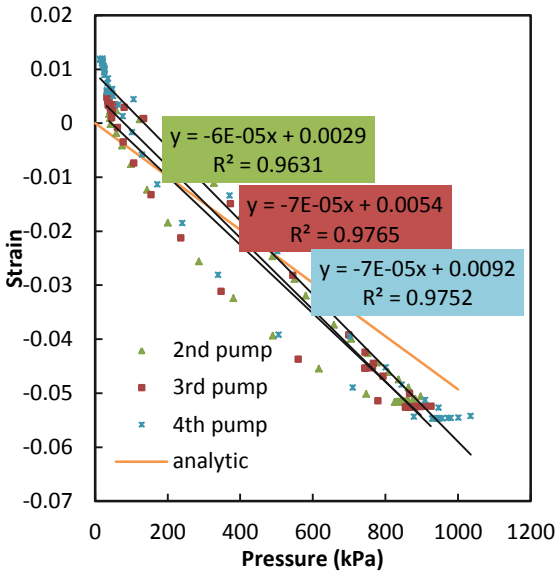

Figure **2-5**: 35° thin-walled free strain.

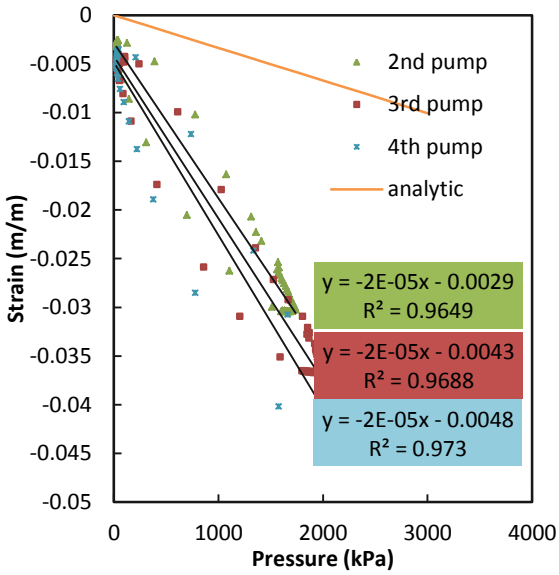

Figure **2-6**: 35° thick-walled free strain.

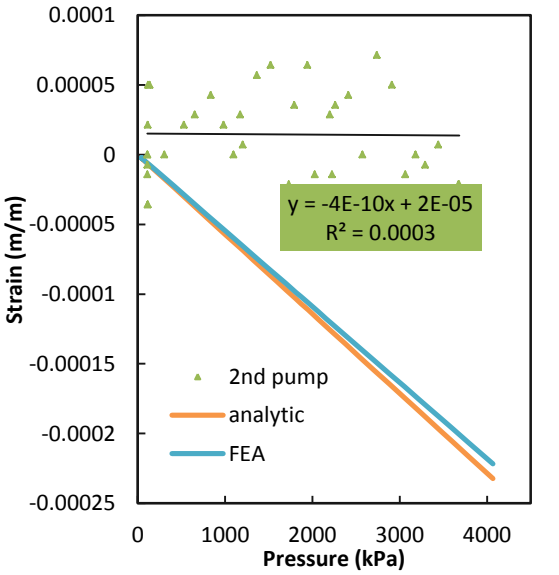

Figure **2-7**: 12.5° bi-layer free strain.

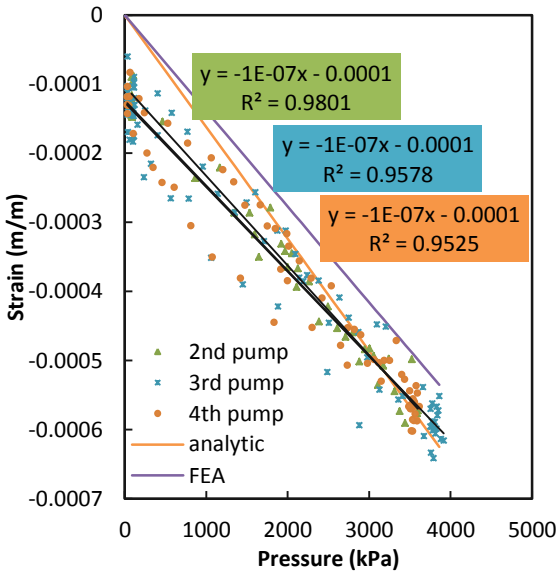

Figure **2-8**: 22.5° bi-layer free strain.

Nonlinearity and shear effects can be seen in Figure **2-9** and Figure **2-10** for the 38.3° and 52.5° bi-layer tubes, respectively. The second, third, and forth pressure cycles all have a small amount of hysteresis but show good repeatability. The slope for the 38.3° specimen is similar to

the predictions, while the slope for the 52.5° specimen is considerably less than the predictions. In Figure **2-10** it is interesting to note that, with each successive pressure cycle, the slope remains the same but the intercept increases. This result is a manifestation of viscoelastic creep in this bi-layer specimen.

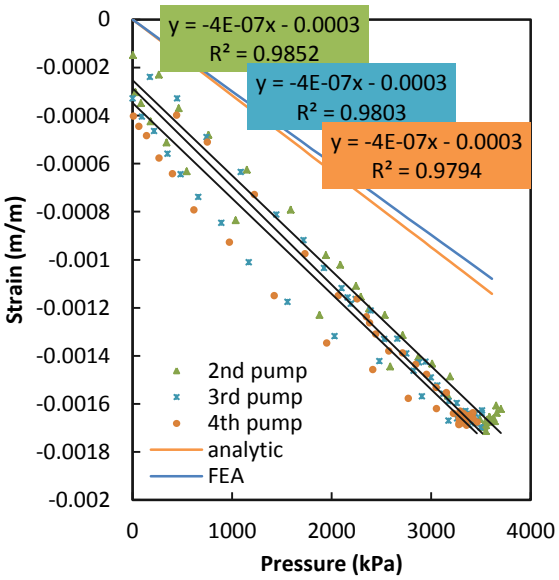

Figure **2-9**: 38.3° bi-layer free strain.

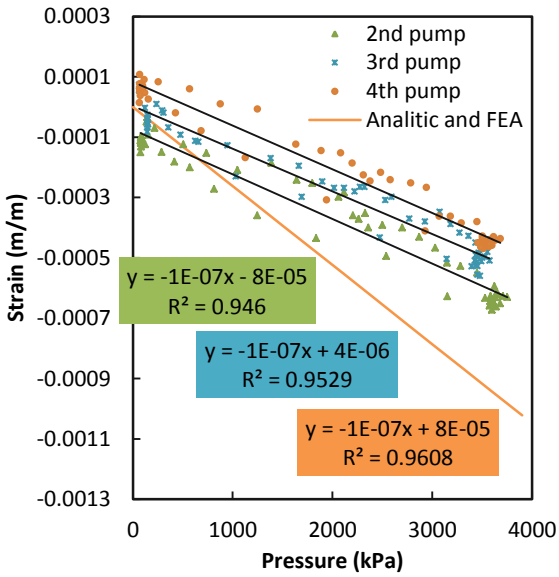

Figure **2-10**: 52.5° bi-layer free strain.

The results of the 62.5° bi-layer specimen are shown in Figure **2-11**. The slope is positive, meaning that this specimen extends with pressurization (all the others contract). This specimen matches the predictions best among all tests. However, as in all the tests mentioned till now, there is significant hysteresis.

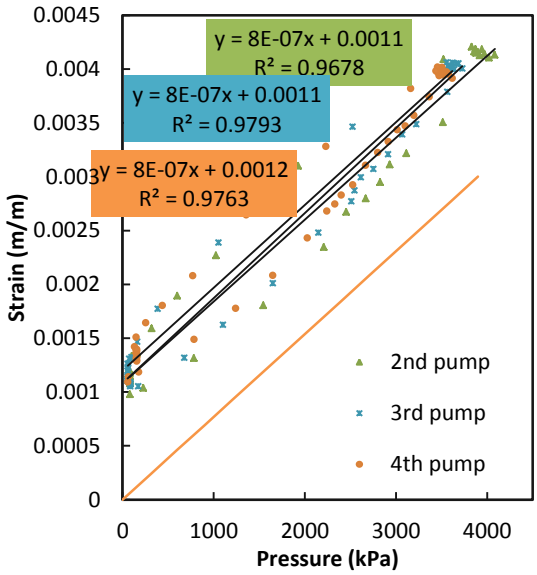

Figure **2-11**: 62.5° bi-layer free strain.

Blocked force

In Figure **2-12** and Figure **2-13**, the blocked force results for the single-layered thin- and thick-walled tubes match almost perfectly with the analytical predictions. In contrast with the free strain tests with the same tubes, there is little to no hysteresis present in the blocked force tests.

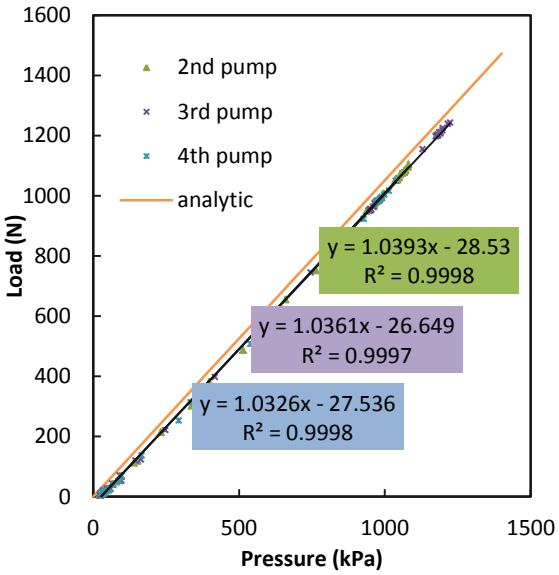

Figure **2-12**: 35° thin-walled blocked force.

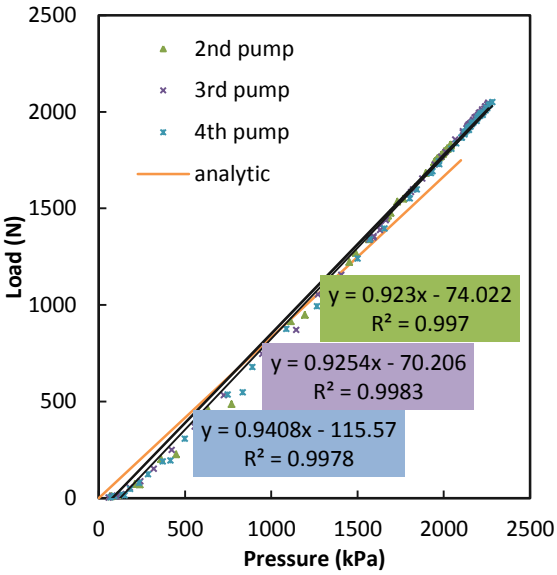

Figure **2-13**: 35° thick-walled blocked force.

For the low-angle bi-layer specimens, the blocked force results are quite divergent from the predictions. In Figure **2-14** the negative slope for the 12.5° specimen suggests that the actuator is extending instead of contracting as predicted. A large difference between the FEA and analytical predictions suggests large end effects in this specimen. In Figure **2-15**, the 22.5° specimen shows high nonlinearity and hysteresis, and hardly any actuation in comparison to the predictions.

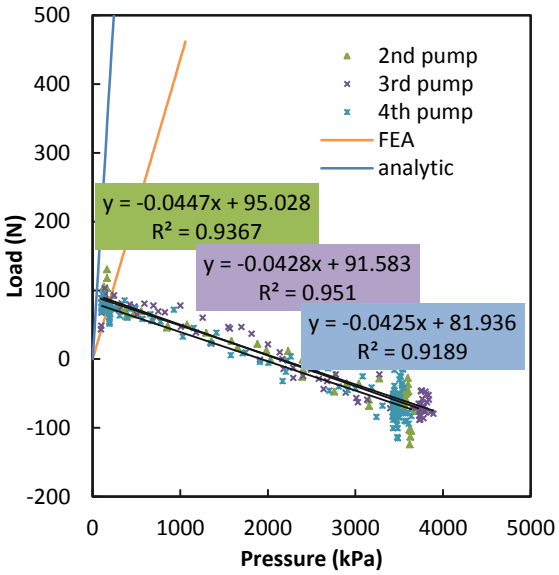

Figure **2-14**: 12.5° bi-layer blocked force.

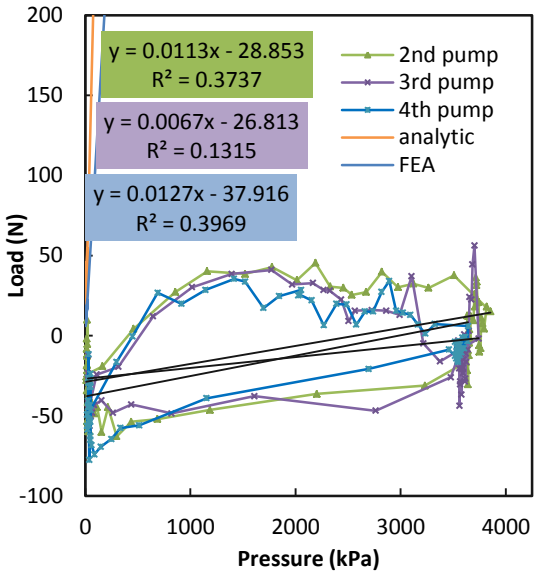

Figure **2-15**: 22.5° bi-layer blocked force.

Additional unexpected results are seen in Figure **2-16** for the 38.3° bi-layer specimen. It appears as though the very first portion of the data matches the predictions closely. However, there is a subsequent region of relaxation where load stays relatively constant as pressure increases. In the 52.5° bi-layer specimen in Figure **2-17**, the data are relatively linear but show only about one-third the slope predicted by FEA and analysis.

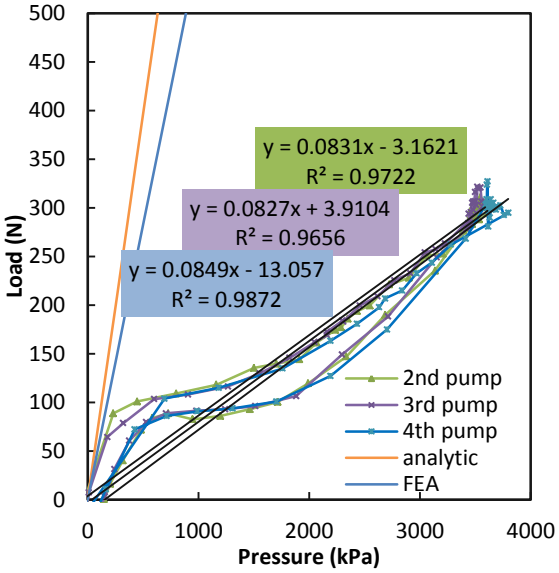

Figure **2-16**: 38.3° bi-layer blocked force.

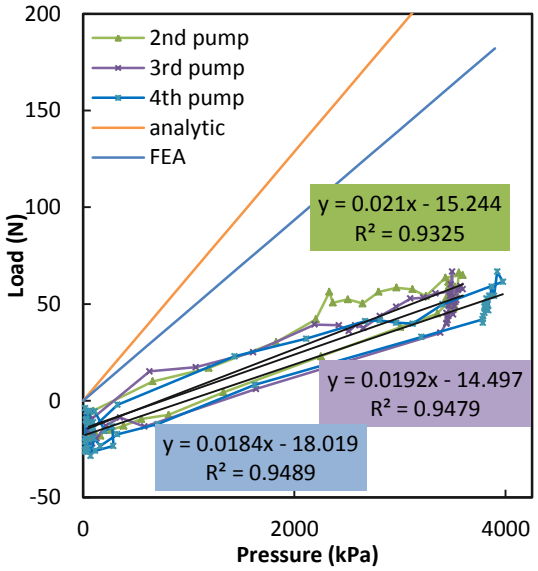

Figure **2-17**: 52.5° bi-layer blocked force.

In Figure **2-18**, the 62.5° bi-layer specimen is the most linear of all in blocked force testing and matches the predictions very well compared with the other bi-layer specimens. Unlike the others, this specimen extends axially with pressurization, producing compressive blocked force as expected.

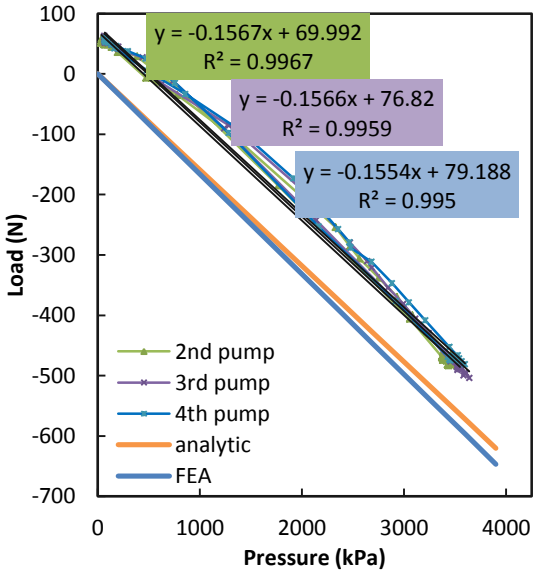

Figure **2-18**: 62.5° bi-layer blocked force.

Axial Modulus

In the axial modulus tests of bi-layer specimens, most of the experimental results matched well with predictions. Results for the two lowest angle specimens were omitted due to small strains that could not be measured with the conservatively limited axial load. As seen in Figure **2-19**, **2-20**, and **2-21**, all of the specimens show a small amount of nonlinearity.

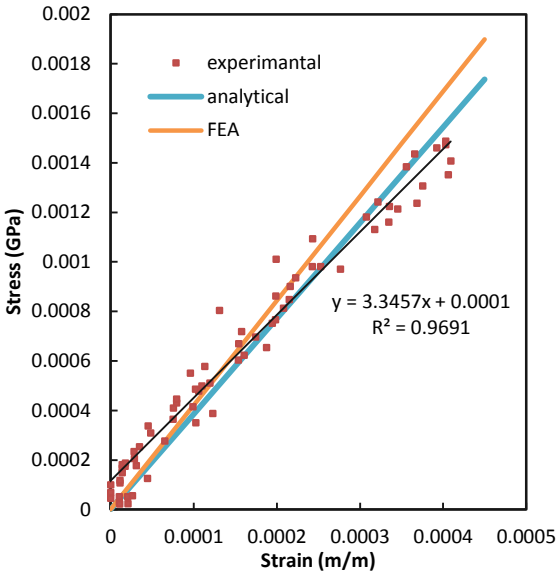

Figure **2-19**: 38.3° bi-layer axial modulus.

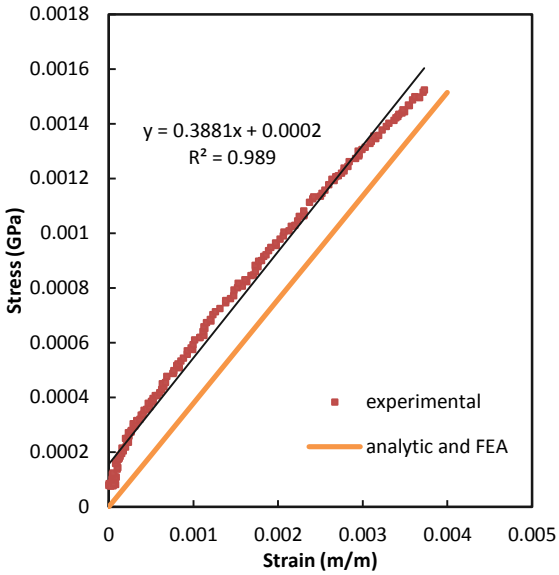

Figure **2-20**: 52.5° bi-layer axial modulus.

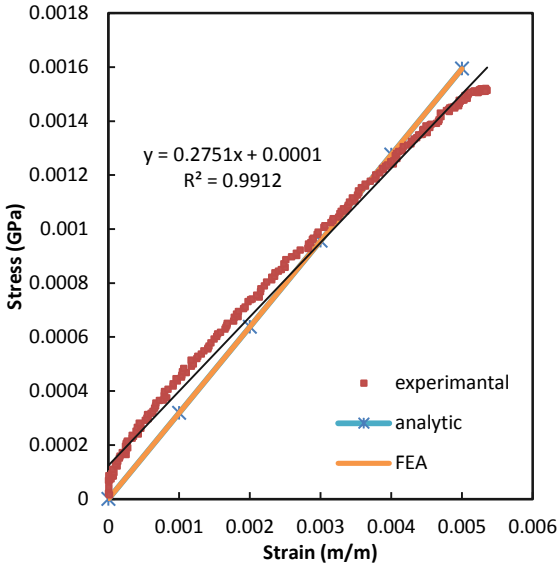

Figure **2-21**: 62.5° bi-layer axial modulus.

Quantitative results

Based on the graphical results presented in the previous sections, Table **2-3** quantitatively compares the slopes of the experiments, analysis, and FEA. In general, the higher angle bi-layer tubes match the predictions better than the lower angle tubes. The 12.5° and 22.5° bi-layer tubes were too stiff to get an accurate axial modulus due to conservatively limited tensile loads on the end plugs.

Table **2-3**: Quantitative summary of results for large tubes.

Tube		Free Strain Slope (1/KPa)	Blocked Force Slope (N/KPa)	Axial Modulus (GPa)
35° Thin	Averaged experimental	-6.60E-05	1.03	N/A
	Analytical	-4.94E-05	1.05	N/A
	FEA	N/A	N/A	N/A
35° Thick	Averaged experimental	-1.67E-05	0.92	N/A
	Analytical	-3.35E-06	0.833	N/A
	FEA	N/A	N/A	N/A
12.5° Bi-layer	Averaged experimental	0	-0.0445	N/A
	Analytical	-5.71E-08	2.07	55.8
	FEA	-5.45E-08	0.436	146
22.5° Bi-layer	Averaged experimental	-1.25E-07	0.0127	N/A
	Analytical	-1.62E-07	2.68	25.5
	FEA	-1.39E-07	1.10	37.7
38.3° Bi-layer	Averaged experimental	-4.01E-07	0.0836	3.35
	Analytical	-3.16E-07	0.791	3.86
	FEA	-2.99E-07	0.565	4.22
52.5° Bi-layer	Averaged experimental	-1.45E-07	0.0194	0.388
	Analytical	-2.62E-07	0.0643	0.379
	FEA	-2.62E-07	0.0467	0.380
62.5° Bi-layer	Averaged experimental	7.73E-07	-0.156	0.275
	Analytical	7.69E-07	-0.159	0.319
	FEA	7.70E-07	-0.166	0.319

Comparing the slopes from the 35° single-layer thin and thick tubes provides insights on the effect of FMC tube thickness on actuation response. In terms of free strain slopes, the thick tube is predicted by analysis to have about 6% of the slope of the thin tube, as one might expect from the 4.5 times greater thickness of the thick tube. Experimentally, the thick tube had a free strain slope 25% of that of the thick tube. Therefore, the measured thickness effect was slightly less than that predicted in free strain response. In terms of blocked force slopes, the thick tube is predicted by analysis to generate about 79% of the slope of the thin tube, while experimentally

the percentage was 89%. Again, the measured thickness effect was slightly less than the predicted effect for blocked forced response.

Comparing the thick 35° tube and the 38.3° bi-layer tube provides insights on the effects of constraint by the surrounding medium. In terms of free strain slopes, the bi-layer tube is predicted by analysis to have about 9% of the slope of the single-layer tube, while experimentally the percentage was found to be 2%. In terms of blocked force slopes, the bi-layer tube is predicted by analysis to generate about 95% of the slope of the single-layer tube, while experimentally the percentage was only 9%. Therefore, for both free strain and blocked force, the measured constraint effect exceeded that predicted by analysis.

A graphical summary of the free strain versus pressure slopes for the bi-layer specimens is shown in Figure **2-22**. The experimental results generally match best with the FEA predictions, but the agreement with the analysis is reasonably good, as well. The blocked force versus pressure slopes for the bi-layer specimens are shown in Figure **2-23**. These experimental results are all less than predicted. Only the 52.5° and 62.5° bi-layer tubes match the predictions well. The main cause of the disagreement is believed to be a problem transferring load from the specimen to the steel end fittings due to shear lag in the soft inner layer. The FEA captures some of this effect.

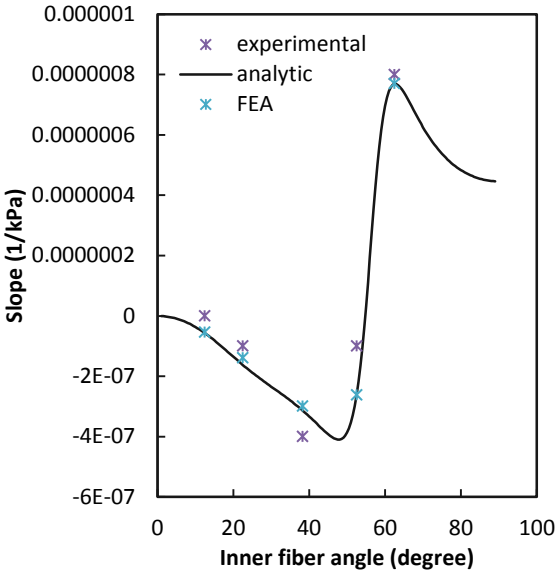

Figure **2-22**: Free strain slopes.

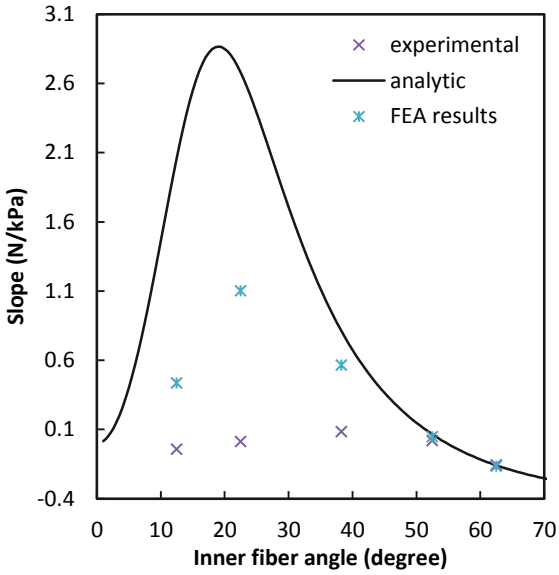

Figure **2-23**: Blocked force slopes.

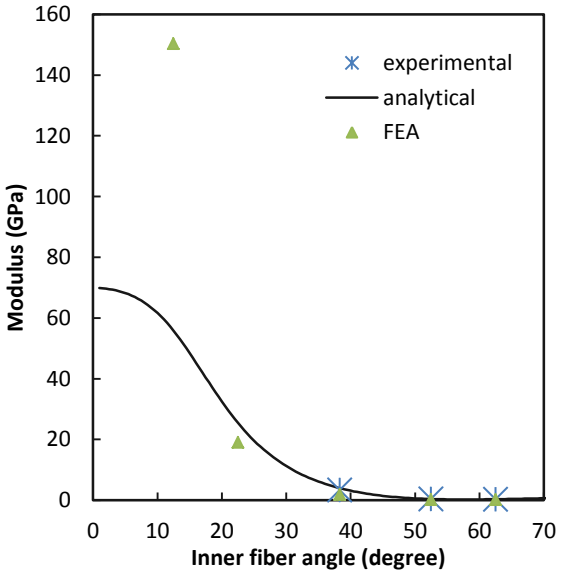

Figure **2-24**: Axial modulus results.

In Figure **2-24**, the axial modulus results from the bi-layer tubes are shown. As mentioned previously, the lower-angled tubes have been omitted from the comparison due to the

high stiffness of the tubes and the low axial load limitation of the end fittings. For the higher angle tubes shown, the modulus matches well with the predictions by analysis and FEA.

Conclusions and recommendations

In free strain experiments, F^2MC actuators of several different fiber angles were shown to deform a surrounding medium in good accordance with predictions. For the material parameters of the present investigation, the free strain per unit pressure decreased by about 1/50 when an actuator with a roughly 35° fiber angle was embedded in a surrounding medium. These results highlight the expected necessity of operating an F^2MC actuation system for morphing structures at pressures exceeding the 4 MPa limit that was conservatively set in the present investigation.

In blocked force experiments involving several different F^2MC actuators embedded in a surrounding medium, the axial forces generated per unit pressure were in significant disagreement with predictions, and in one case had opposite sign. These disagreements are believed to be due to material nonlinearity, viscoelastic deformation, and end effects such as shear lag between the inner layer and the steel plugs as well as the outer layer near the ends of the specimen. A reduction factor in axial force per unit pressure of roughly 1/10 was measured when embedding an actuator of roughly 35° fiber angle into a medium.

Additional experiments are recommended to generalize these results for other fiber angles in the F^2MC actuators and other stiffnesses of surrounding media. Detailed evaluation of the three-dimensional constitutive behavior of the FMC material, possibly including the nonlinear effects of fiber undulations created by filament winding and viscoelastic effects, are recommended as well.

Chapter 3

FMC Integrated with Structures

Introduction

The original idea of evaluating the performance of an F^2MC tube embedded into a relatively rigid structural medium was to cast it into epoxy. It was decided that such a specimen might be difficult to manufacture. Therefore, an outer layer of filament wound composite with an axial stiffness and Poisson's ratio similar to epoxy was selected for the experiments discussed in Chapter 2. After carrying out the experiments of Chapter 2 and suspecting significant end effects due to out-of-plane shear deformation in the thick-walled FMC tubes, it was decided to return to the idea of casting the tube in an isotropic medium where the out-of-plane shear modulus of the outer layer is not tremendously less than the axial modulus. The first attempt involved the casting of an epoxy outer layer around a thick-walled FMC tube. The ends of the FMC tube were sealed off and it was placed inside of a mold consisting of a PVC tube. The inner diameter of the PVC tube corresponded to the desired outer diameter of the epoxy layer. Release spray was used so that the tube would not bond to the epoxy casting. This approach had many problems as can be seen in a photograph of the resulting specimen in Figure **3-1**.

Figure **3-1**: Photograph of thick FMC tube cast in epoxy.

The first and biggest problem was believed to be due to cure shrinkage of the epoxy creating large voids and cracks in the epoxy. The second problem can also be seen in the photograph is that the release spray did not work well and the PVC tube was bonded to the epoxy in places, creating a lot of work to remove it from the tube. These cleaning attempts also caused some damage to the epoxy casting. This approach was therefore abandoned, and it was decided to bond a pre-cured polycarbonate outer tube to another thick-walled FMC tube.

Experimentation

Materials

The AS4/Reoflex 20 FMC actuator tube is the same as the 35° thick tube described Chapter 2. The outer diameter is 30 mm. The FMC tube was bonded with epoxy inside a polycarbonate tube with a claimed modulus of 2 GPa and Poisson's ratio of 0.37. The

polycarbonate inner diameter and outer diameters are 30 mm and 38.1mm, respectively. The unidirectional composite properties of the FMC tube are the same as given previously for AS4/Reo 20 in Table **2-1** in Chapter 2. These properties were again used by Mr. Bin Zhu to run an analytical elasticity-based solution for infinitely long orthotropic tubes to generate predicted specimen performance under testing. The actual length of the FMC tube was approximately 305 mm while the length of the polycarbonate tube was approximately 220 mm.

Manufacturing method

As previously described in Chapter 2, the FMC tube was filament wound using AS4/Reoflex 20. To bond the FMC tube to the polycarbonate tube, the surface of the FMC tube was first prepared to create a good bond surface. This was accomplished by using an acetone soaked paper towel to lightly clean the surface and strip some of the outer layer of polyurethane off to expose some fibers. Water was used to clean the polycarbonate tube as acetone would degrade the surface and create a hazy, gritty surface. Next, a general purpose two part epoxy (Hardman Double Bubble Extra Fast Setting Epoxy, Red Pkg., Royal Adhesives and Sealants LLC, South Bend, IN) was mixed and applied to the inner surface of the polycarbonate tube and the outer surface of the FMC tube. Then, the polycarbonate tube was carefully slid onto the FMC tube, gently spinning it to spread the epoxy throughout the bonded interface. Once the FMC tube was in place, a syringe was used to inject additional epoxy to fill in open spaces near the ends and to push out air remaining air pockets. After the specimen cured at room temperature, there was still some space in the tube where epoxy ran out that needed to be filled with epoxy. To do this, a hole was drilled into the polycarbonate tube and epoxy injected to fill in the void. The final product can be seen in Figure **3-2**. To prepare the specimen for testing, hose clamps were applied

to the uncovered section of the FMC tube to clamp down on the pipe fittings that were bonded inside the FMC tube using the same methods and epoxy as described in Chapter 2.

Figure **3-2**: FMC tube bonded into a polycarbonate tube, with threaded end fitting in place.

Tests

The same three types of tests were carried out to characterize the mechanical behavior of the specimen: free strain, blocked force, and axial modulus. Each of these tests was repeated twice with teardowns in-between to ensure repeatability of the results. The procedure for these tests was described in detail in Chapter 2. The test apparatus and setup were all the same along with the ranges and calibrations. The free length used for strain calculations between the bonded fittings of the tube was measured to be 220 mm.

Results

Free Strain

Analytic results for the bonded F^{2}MC tube were generated by Mr. Bin Zhu. It should also be noted that, like in all the tests run on F^{2}MC tubes, the first out of four pressurization cycles has been removed so that any softening of the tube will not affect results (e.g., the Mullins effect [12]). The two free strain test runs are shown in Figures **3-3** and **3-4**. The experimental results match very well with predictions, as was the case with bi-layer FMC tubes. It is also seen that this tube preforms as expected as a contractor tube by having negative strains. The bonded tube only differs from the bi-layer tube by showing little to no hysteresis. This is likely due to the polycarbonate tube restraining radial and axial movement of the FMC with less effects of the low out-of-plane shear modulus of the FMC material. Repeatability between the two tests is excellent.

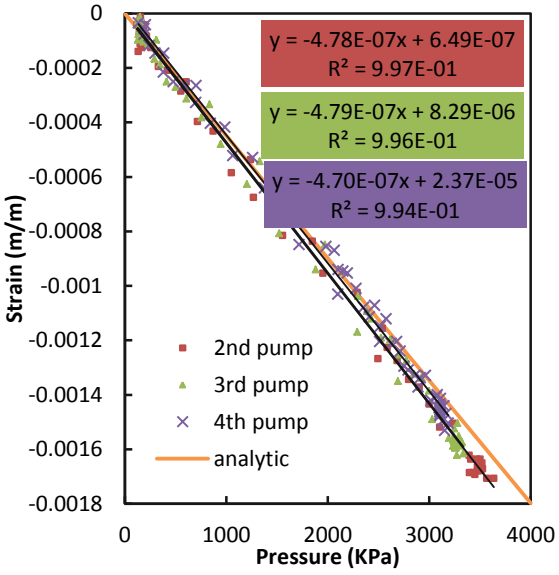

Figure **3-3**: Bonded tube free strain test #1.

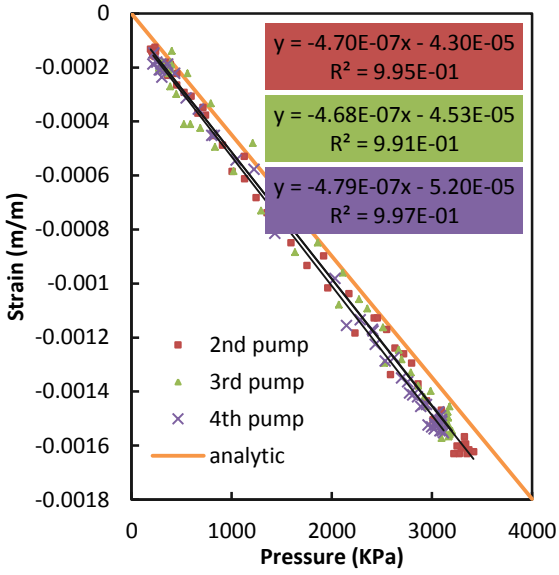

Figure **3-4**: Bonded tube free strain test #2.

Blocked Force

As was seen with the bi-layer tubes tested for blocked force, the bonded tube results shown in Figures **3-5** and **3-6** underperform the predictions. The results are repeatable between the first and second tests. The conclusion is that, again, poor load transfer at the end fittings to the testing frame and shear lag between inner and outer layers is causing these lower than expected slopes. Also, much hysteresis was present in the pressurization cycles, as was seen in the bi-layer tube tests.

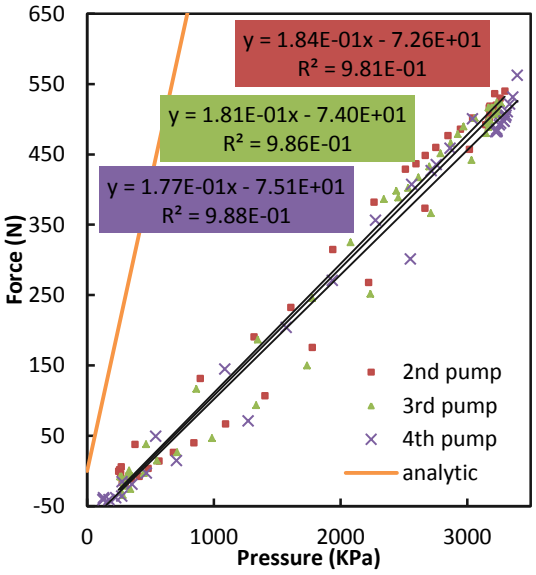

Figure **3-5**: Bonded tube blocked force test #2.

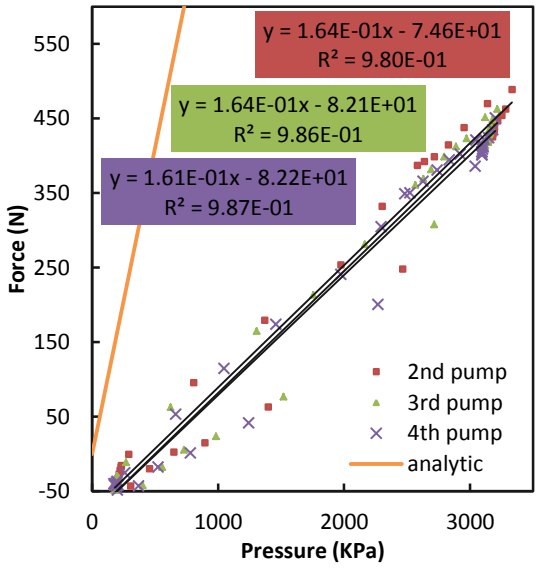

Figure **3-6**: Bonded tube blocked force test #2.

Axial Modulus

Figures **3-7** and **3-8** show that the axial modulus tests match the predictions well and are consistent in repeated tests. These results are consistent with the bi-layer tube test results.

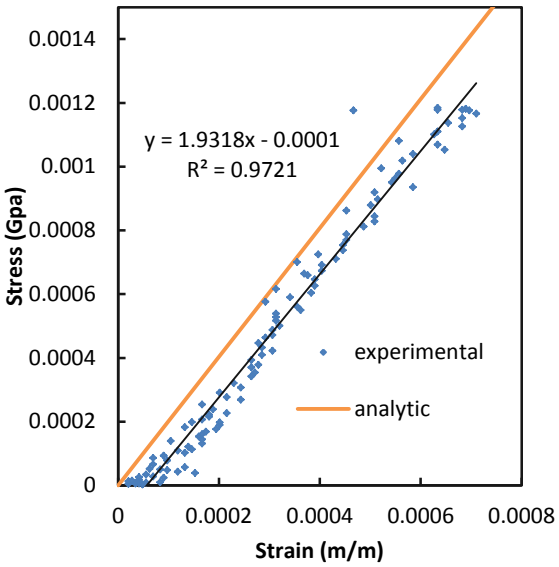

Figure **3-7**: Bonded tube axial modulus test #1.

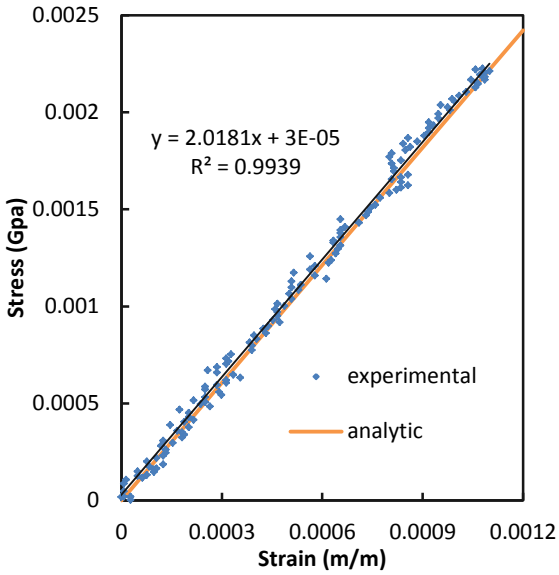

Figure **3-8**: Bonded tube axial modulus test #2.

Quantitative results

Based on the graphical results presented in the previous sections, Table **3-1** quantitatively compares the slopes of the experiments and analysis. It also shows the 35° thick and thin tubes as a comparison to the bonded thick tube. Comparing all the results, it is clear that bonding the thick tube into a stiff medium such as polycarbonate reduces the free strain and blocked force as can be expected. It can also be seen that although the difference between the predicted block forces for 35° thick tube and the bonded tube is negligible, the difference between the corresponding experimental results is significant (about a factor of five).

Table **3-1**: quantitative summary of results.

Tube		Free Strain Slope (1/KPa)	Blocked Force Slope (N/KPa)	Axial Modulus (GPa)
35° Thin	Averaged experimental	-6.60E-05	1.03	N/A
	Analytical	-4.94E-05	1.05	N/A
35° Thick	Averaged experimental	-1.67E-05	0.92	N/A
	Analytical	-3.35E-06	0.833	N/A
35° Thick bonded tube	Averaged experimental	-4.74E-07	0.172	1.97
	Analytical	-4.50E-07	0.8223	2.019

Comparing the slopes gives insight on the effect of casting or bonding a tube into a stiffer material. In terms of free strain slopes, the bonded tube is predicted by analysis to have about 13% of the slope of the thick tube by itself, while experimentally the percentage was found to be 3%. In terms of blocked force slopes, the bonded tube is predicted by analysis to generate about 99% of the slope of the single-layer tube, while experimentally the percentage was only 19%.

Conclusions and recommendations

Again with this tube the free strain results are in good accordance with predictions. There are large underperformances in blocked force common in many FMC's tested in this paper. These problems are believed to be due to shear lag at the ends and viscoelastic deformations. Since the performance of these tubes is so poor for the blocked force tests these tubes would not make very useful actuators as a force would be needed to actuate. Based on difficulty to fabricate these tubes and the large underperformances it is recommended that these type of tubes would not be well suited for use as a rigid actuator.

Start here

Chapter 4

Small Braided Tubes

Introduction

Until recently, F^2MC tubes have been relatively large and bulky now there is a push to examine smaller tubes on the order of a few millimeters. Some ideas for uses of these are embedding into panels but these panels will not be big and bulky like previous concepts and designs [1 and 13]. There is even a concept to take these small diameter tubes and wind them into a tubular type structure and evaluate its characteristics. The goal is to make something that is easy to make and practical to use in a variety of applications. Because of their small diameter (less than 1 cm), these new tubes cannot be readily made by the previous filament winding techniques. Rather, a proven way to make small diameter tubes containing fiber reinforcement is by braiding steel wire over a soft extruded polymer and then extruding another layer of the soft polymer over the inner two layers. Effectively there is an inner layer consisting of a soft matrix material, a middle layer of steel or other fiber type material, and an outer layer of soft matrix material. A company named New England Wire Technologies Corp., through a subsidiary named New England Catheter (Lisbon, NH), makes such tubes for medical catheters. This company was able to manufacture custom tubes for the current investigation.

Experimentation

Materials

Constituents

These tubes can be represented as 3 layers the inner and outer layers are polyurethane and the middle is polyurethane with a reinforced stainless steel wire. The matrix material used was chosen because it was the only material available from the vendor that was close to the same stiffness of polyurethane used in the large tubes. The polyurethane had a variety of ranges for tensile modulus for a given % elongation. The absolute maximum and minimum of 11 MPa and 3.8 MPa (1600psi and 550psi), respectively, were used by Mr. Bin Zhu to analytically predict the performance of the small tubes. The full data sheet as received by New England Wire Technologies Corporation can be found in Appendix A. The stainless steel reinforcement used was a flat 0.0254 mm by 0.1016mm (0.001 by 0.004 in.) type 304v hard stainless steel.

Manufacturing method

Due to proprietary methods used in manufacturing of these tubes, the details of how they were made can only be conjectured. The only information available is that they were made by braiding the reinforcement onto an extruded tube and then using another extrusion process to add the outer layer of polyurethane.

The order was also split into two different braid angles so that the experimental results could be used to better validate the analytical model. The angles of 25° and 35° were chosen because they were both predicted to give easily measurable blocked force and free strain. Figure **4-1** shows the two tubes side by side next to a ruler with an inch scale.

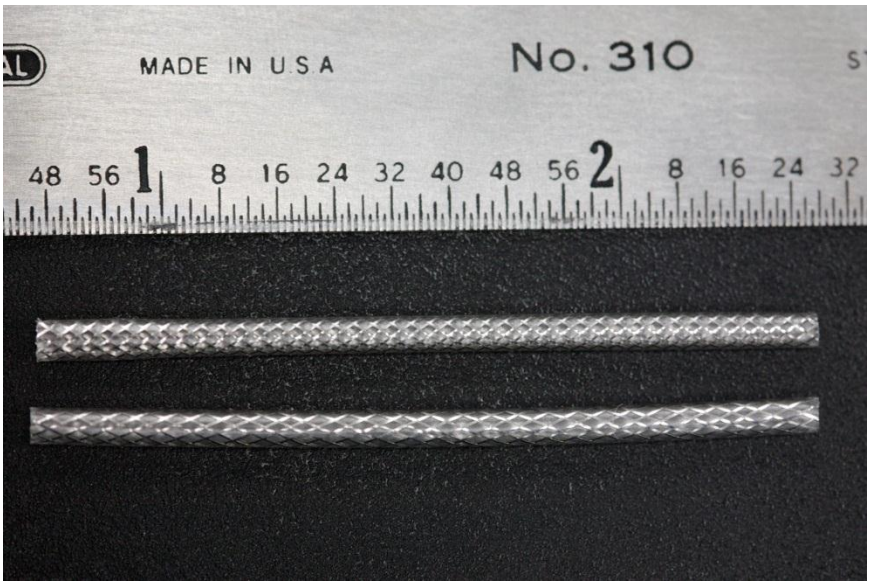

Figure **4-1**: Photograph of small braided tubes.

The dimensions received from the manufacturer's specifications include the inner and outer diameter only. Tube specifications as received from the manufacturer can be found in Appendix A, Figure **A-2** and **A-3**. Due to the small diameters of the tubes only the outer diameter could be verified using a dial calipers for both sets of tubes. The other layer diameters were estimated based on wire thickness. The middle layer was calculated by doubling the wire thickness co account for the areas where the wires overlap. The inner and outer layer dimensions were calculated by dividing up the remainder wall thickness evenly on either side. It was also assumed that the two different angle batches had the same inner layer dimensions based on the same measured outer diameter; the dimensions used for these layers can be seen in Table **4-1**.

Table **4-1**: Layer diameters of small braided tubes.

Layer	Inner diameter (mm)	Outer diameter (mm)
Inner polyurethane	1.65	1.79
Middle reinforced	1.79	1.89
Outer polyurethane	1.89	2.03

In order to estimate the orthotropic elastic properties of the tubes, the volume fractions and properties of the constituent fiber and matrix are needed. The vendor provided only an approximate fiber areal coverage of 55%. To determine the fiber volume fraction, a model of the fibers was created using CAD software (ProEngineer, PTC, Needham MA). A screen shot of this model can be seen in Figure **4-2**. This model represented a unit surface area of the tube that has been unrolled and flattened out. Two layers of the fibers were created to represent the positive and negative fiber directions. The spacing between the fibers was adjusted until there was approximately 55% fiber coverage of the unit area.

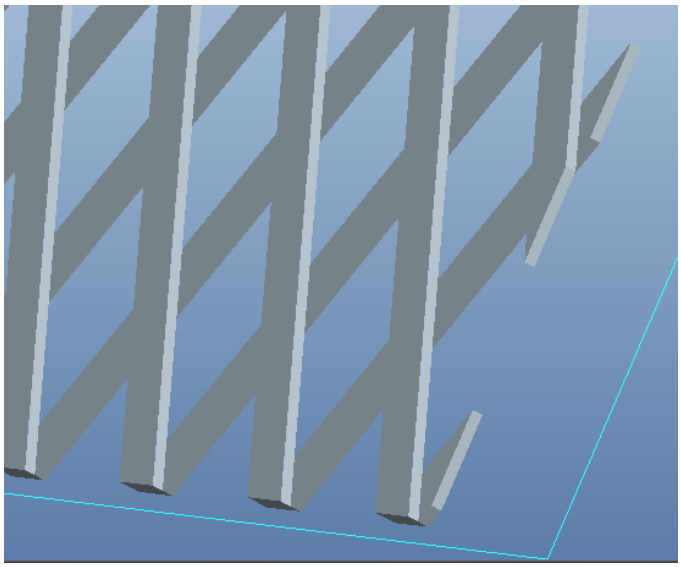

Figure **4-2**: Solid model of fibers in small tubes.

From this model, the total volume of the wires could be calculated in the CAD program. This could then be divided by the total volume of the reinforcement layer since the square containing the wires is a unit area, the total volume of the reinforcement layer is just double the wire thickness. The fiber volume fraction came out to be approximately 26% for the middle layer or about 7% for the total tube. Similar volume fractions were obtained with both braid angles. The maximum and minimum modulus range of 11 MPa and 3.8 MPa and a v_m of 0.5 was assumed for the polyurethane. A modulus of 200 GPa and v_f of 0.3 was assumed stainless steel reinforcement. Using this data, the ply properties shown in Table **4-2** were calculated and used in

the subsequent analysis by Mr. Bin Zhu to predict tube responses for both upper and lower limits of polyurethane stiffness.

Table **4-2**: Calculated unidirectional composite ply properties for the small braided tubes.

Lamina property	Middle reinforced layer (stiffer polyurethane)	Middle reinforced layer (softer polyurethane)
E_{11} (GPa)	52	52
E_{22} (MPa)	18.7	6.47
ν_{12}	0.45	0.45
ν_{23}	0.93	0.93
G_{12} (MPa)	6.24	2.16

The braid angle of the tubes was verified using two methods. The first was to measure the axial distance (L) that that it took for one wire to wrap 360° around the tube and also the circumference (C) of the layer containing the reinforcement. The mean diameter of 1.84 mm for the middle layer was used to calculate the circumference. The L quantity was measured within ±1/64 of an inch. Equation (4-1) was used to calculate the angle for both kinds of braided tube.

$$\theta = \frac{180}{\pi}\tan^{-1}\left(C/L\right) \tag{4-1}$$

The angle for the larger angle tubes was calculated to be 39°-42°, while for the smaller angle tubes it was 23°-24.5°. The angles used in the predictions of material behavior were taken as 40° and 24°.

The second method used to verify the braid angle was to take pictures of the braiding under magnification and using trigonometry, calculate the braid angle based on pixel locations. Pixels were chosen near the center of the tube which shows as the white shiny area in Figures **4-3** and **4-4**. This was done because points taken at other places on the tube would not give an

accurate fiber angle due to curvature of the tube. This method proved to be an inaccurate way to calculate braid angle, with variations in calculated angle of a few degrees. However it did prove useful as a way to verify that the first method was giving similar angles.

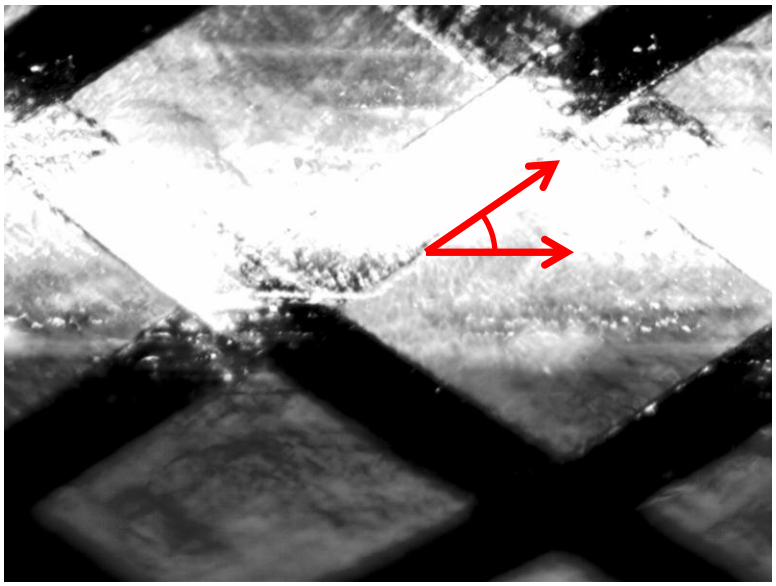

Figure **4-3**: Photomicrograph of higher angle braided tube.

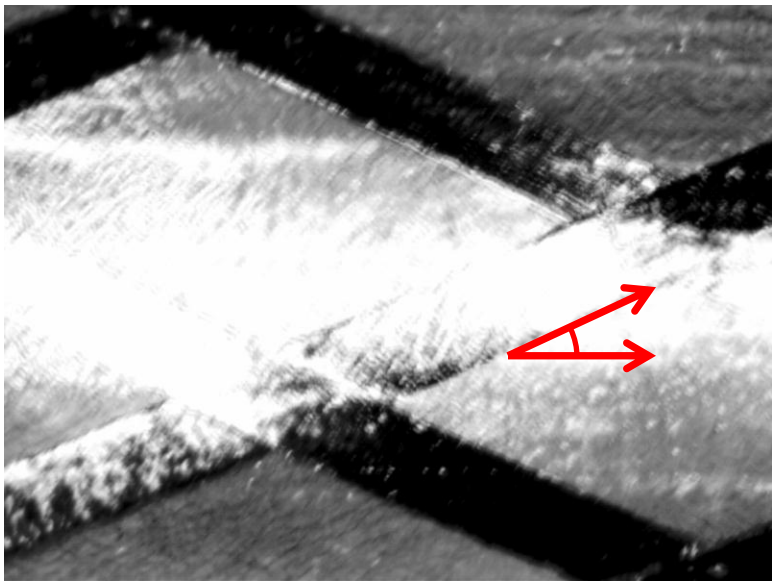

Figure **4-4**: Photomicrograph of lower angle braided tube.

Due to the small diameter of the braided tubes, the general method developed for attaching end fittings to the large tubes in Chapter 2 was considered infeasible for the braided tubes developed. Therefore, a different concept based on a blind NPT pipe plug was adopted. The pipe plug was drilled out as illustrated in Figure **4-5**. The portion of the hole at the "back end" of the plug was drilled with a larger diameter than the "front end" so that the two part methacrylate adhesive, Devcon Plastic Welder (ITW Devcon, Danvers MA) used to bond the tube would form a mechanical bond with the plug rather than just relying on an interfacial bond. The arrow in the lower right diagram of Figure **4-5** indicates the direction that the tube is pulled during a tensile test.

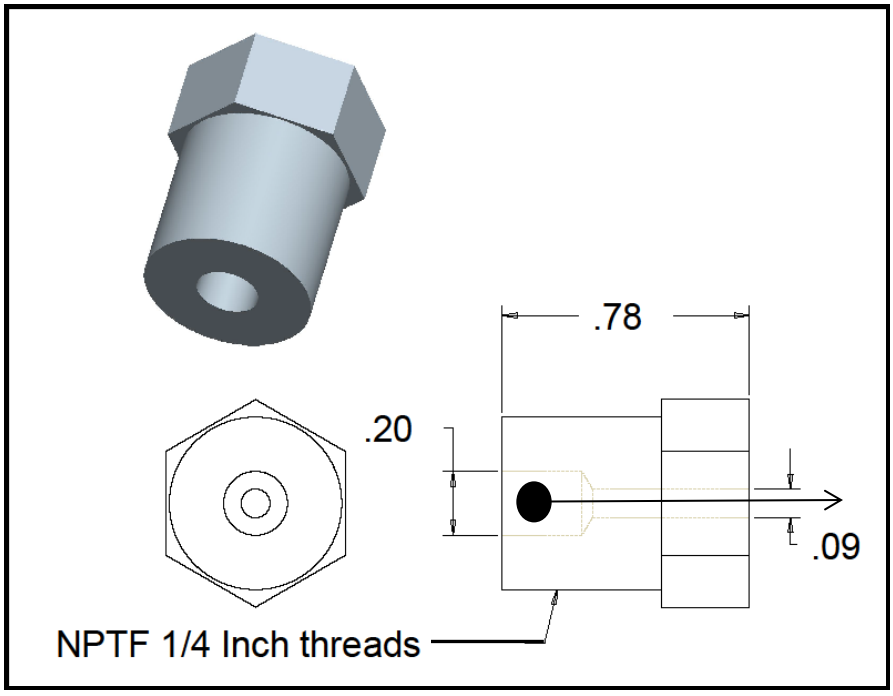

Figure **4-5**: Diagram of steel plug used as an end fitting for the braided tubes.

To prepare the tubes for bonding, they were first cut to desired length which included desired testing gauge length and extra to account for the length bonded into fittings. The tubes were carefully cut using a sharp razor with a light sawing motion being careful to not kink or

smash the tubes during cutting. The surfaces that were to be bonded into the plugs were wiped down lightly with an acetone soaked paper towel until they had a slight haze. It was also important to clean the fitting after each use because of the decision to burn out the previously tested tube, which left some debris inside the bore of the fitting. The outside of each fitting was cleaned using a wire wheel and the inside was cleaned using the same drills that were used to drill the two bores through the fitting. Then, small twisted up pieces of paper towel soaked with acetone were passed through the hole until they no longer came out dirty. A two part methacrylate adhesive, Devcon Plastic Welder (ITW Devcon, Danvers MA) was used to bond the tubes into the fittings. For the bonding operation, the fittings were first slipped over both ends of the tube. The adhesive was then mixed and applied to the ends of the tube. The, the two fittings were slid towards the opposite ends of the tube until they reached their final intended positions. The fittings were spun during this insertion process to allow the adhesive to completely cover the interface between tube and fitting. Insertion of the tubes into the fittings had to be done carefully so that the tubes would not get bent and kinked. It was also useful to apply the Teflon tape to the fitting threads before bonding it to the tube not only for sealing the threads for pressurization tests but also to enable the easy removal of excess adhesive from the threads. A fillet of adhesive was also applied at the tube/fitting junction on the end facing the gage section, as seen on the right side of the fitting in Figure **4-6**. Once adhesive was cured the final gauge length was then measured between the fillets using a calipers.

Figure **4-6**: Photograph of end fitting bonded to a small braided tube.

In two rounds of testing, some specimens showed signs of slipping based on the test results, even though no physical signs of slippage could be observed from the specimens after testing. While preparing fittings for a new set of tubes, it was seen that sometimes when pulling the tubes out that the polyurethane remained bonded into fittings while the wire reinforcement pulled out. It was theorized that some of the slipping could be due to the wire itself slipping inside the polyurethane reinforcement since there did not seem to be a strong chemical bond between the wire and the polyurethane. It was decided to try a different method for bonding the tubes on a third set of tests to directly connect the steel wire to the end fittings. To expose the wire, a method to strip the polyurethane from the tube was developed. First, the end was soaked in acetone for approximately 45-60 seconds. After soaking, the polyurethane would be soft and could then be stripped off using finger nails or a dull scraping tool. Repeated soakings were needed sometimes to remove any leftover polyurethane until the tubes appeared as shown in Figure **4-7**.

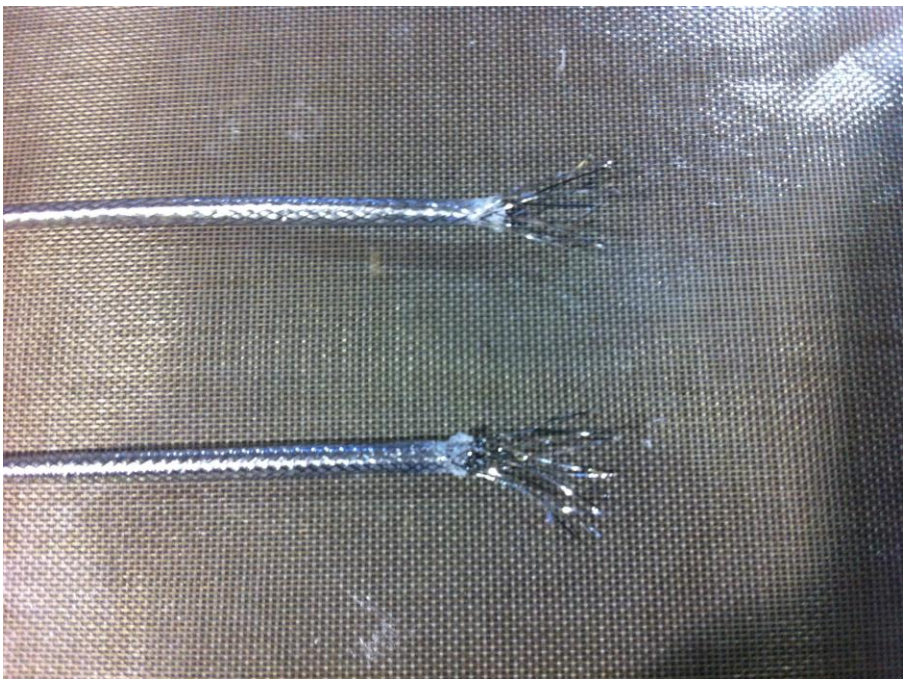

Figure **4-7**: Photograph of polyurethane striped from ends of braided tubes.

Once the wire was exposed, it was then carefully bent back down around the tube as shown in Figure **4-8**. To bond the tube into the end fittings, adhesive was applied to the end of the tube and the exposed wire as was described earlier. When sliding the fitting down the tube, the wire embedded into the adhesive and became directly engaged in the adhesive bond along with the outer layer of polyurethane.

Figure **4-8**: Photograph of exposed wire reinforcement prior to attaching end fittings for the third round of braided tube tests.

A few more final preparations were needed to ensure the tubes and fittings were ready for testing. First was to inspect the bonds for any obvious sealing issues or imperfections that could cause premature failure. The second was to make sure the adhesive is clear of the threads. If not, the adhesive was removed using a razor blade or wire wheel and the Teflon tape was re-applied to the threads. The third is to make sure that no adhesive got into the tube so fluid may pass though the tube during pressurization cycles. If the tube was plugged with the adhesive, it could sometimes be removed by using a razor blade to cut away the excess otherwise the tube had to be removed from both fittings and entire process of attaching a fresh tube to the fittings had to be repeated.

Tests

Three types of tests were carried out to characterize the mechanical behavior of the braided specimens: free strain, blocked force, and axial modulus. The testing apparatus included a servo-hydraulic load frame into which the specimens could be pinned through the end fittings, a hand-pump, strain gage based extensometers, and an electronic pressure transducer. The load frame was equipped with a 1.3 kN load cell and an actuator with a 150-mm stroke. The hydraulic hand pump was limited to 700 KPa to prevent blowouts. The tube shown in Figure **4-9** blew out in the gap between reinforcement at a pressure of approximately 1100 KPa.

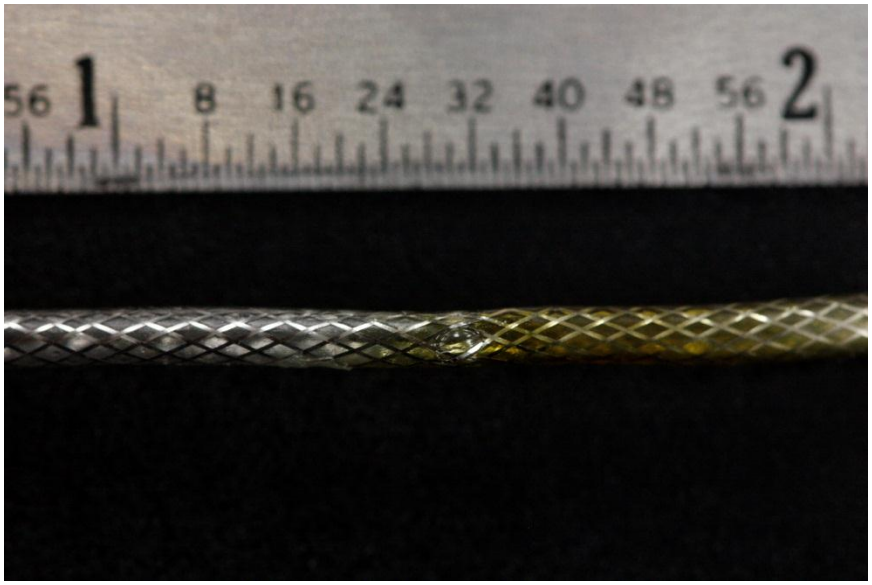

Figure **4-9**: Photograph of a blown out braided tube.

The three different test setups for the three types of tests are shown in Figures **4-10** and **4-11**. Since the end fittings had to be threaded into the load train, swiveling hydraulic fittings were used to prevent twist-up of the tubes during insertion into the load train. The top fitting was tightened first so that the tube could hang freely. For the free strain tests, a dial pressure gauge was then threaded to the bottom end of the tube. Because these tubes were too small to put the

extensometer directly on tube surface, one arm of the extensometer was attached to the free end fitting and the other arm was held motionless relative to the load frame, as shown in Figure **4-10**. Therefore, the extensometer measures the change in length of the entire tube by measuring how far the free end moves during pressure cycles. As with the bi-layer tube experiments, the first of four pressure cycles was discarded and the recorded results were confined to the second, third, and fourth cycles. For each pressurization/depressurization cycle, the axial strain versus pressure slope was found by fitting a straight line by the least-squares method to the entire cycle. The final strain versus pressure slope assigned to each test was found by averaging the slopes from the last three pressure cycles. Several sets of tests were conducted using varying lengths of tubes to check for end effects and consistency. The corresponding designation for specific lengths can be found in Table **4-3**. For example a graph labeled B-3 represents the third tube tested in the 96 mm gauge length set for the designated braid angle. For the shortest tube lengths (A), a total of four different tubes per braid angle were tested. A total of two different tubes per braid angle were tested for the other two longer test lengths (B and C).

Table **4-3**: Gauge length designations.

Tube test length designation	Tube gauge length (mm)
A	56
B	96
C	85

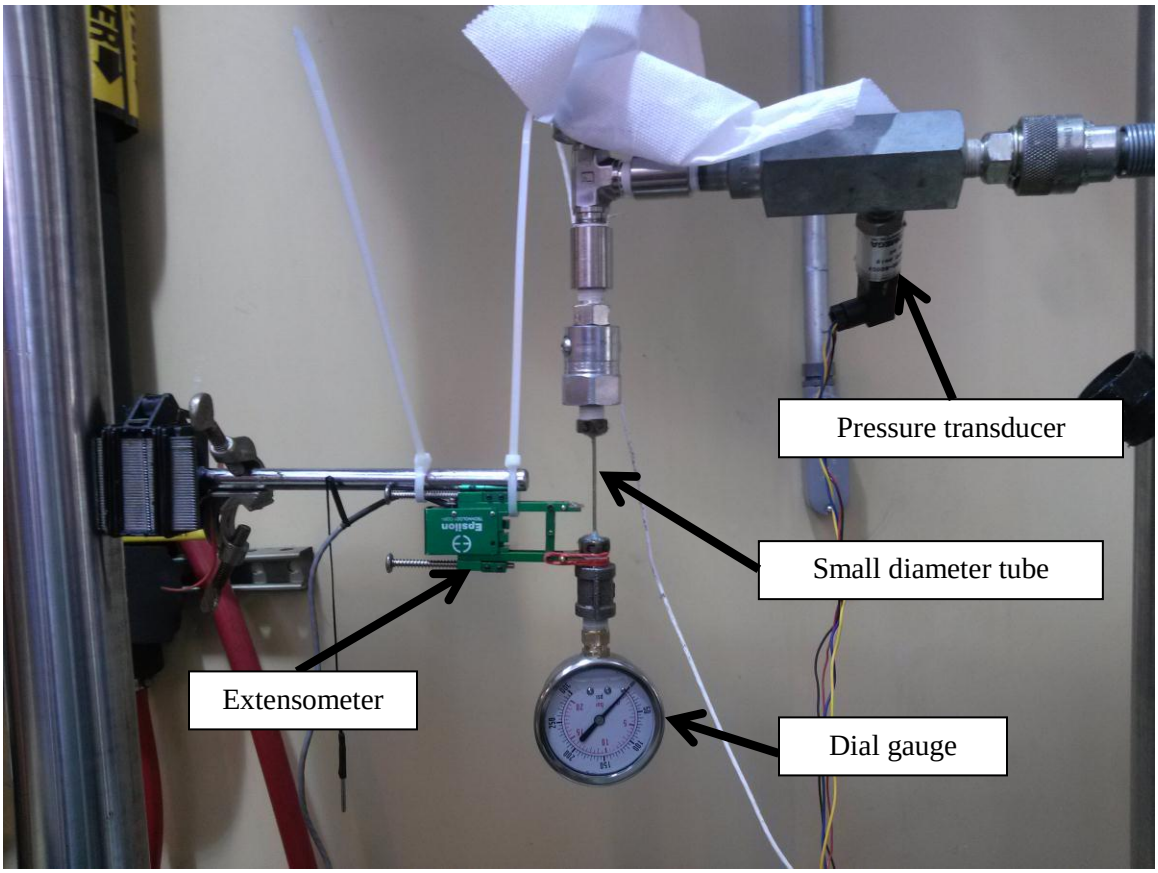

Figure **4-10**: Free strain test setup for braided tubes.

Figure **4-11** shows the setup for the blocked force and axial modulus tests. For these two tests, the setup is basically the same except that for the axial modulus test the hydraulic pump is disconnected and all fluid is drained from the tube. The upper end of the tube was attached the same way as for the free strain tests. The bottom end was attached by carefully adjusting the position of the hydraulic actuator while simultaneously threading the fitting. While threading the fitting, it was important to not bend or twist the tube too much to avoid permanent deformation.

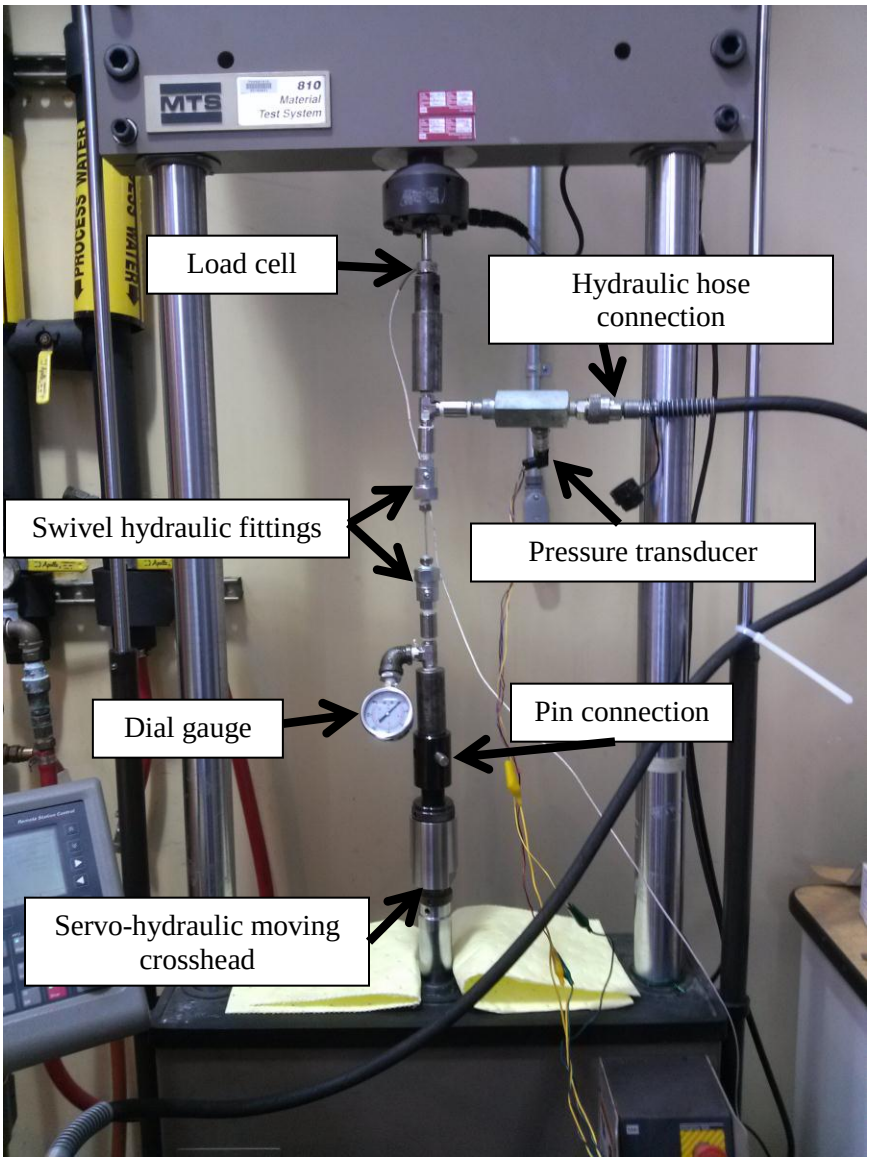

Figure **4-11**: Blocked force and axial modulus test setup for braided tubes.

Figure **4-12** shows a closer view of the blocked force and axial modulus test setup. The tube threaded into the swivel fittings pinned into the load frame. The dial gauge is used for reference when pressurizing using the hand powered hydraulic pump not pictured here.

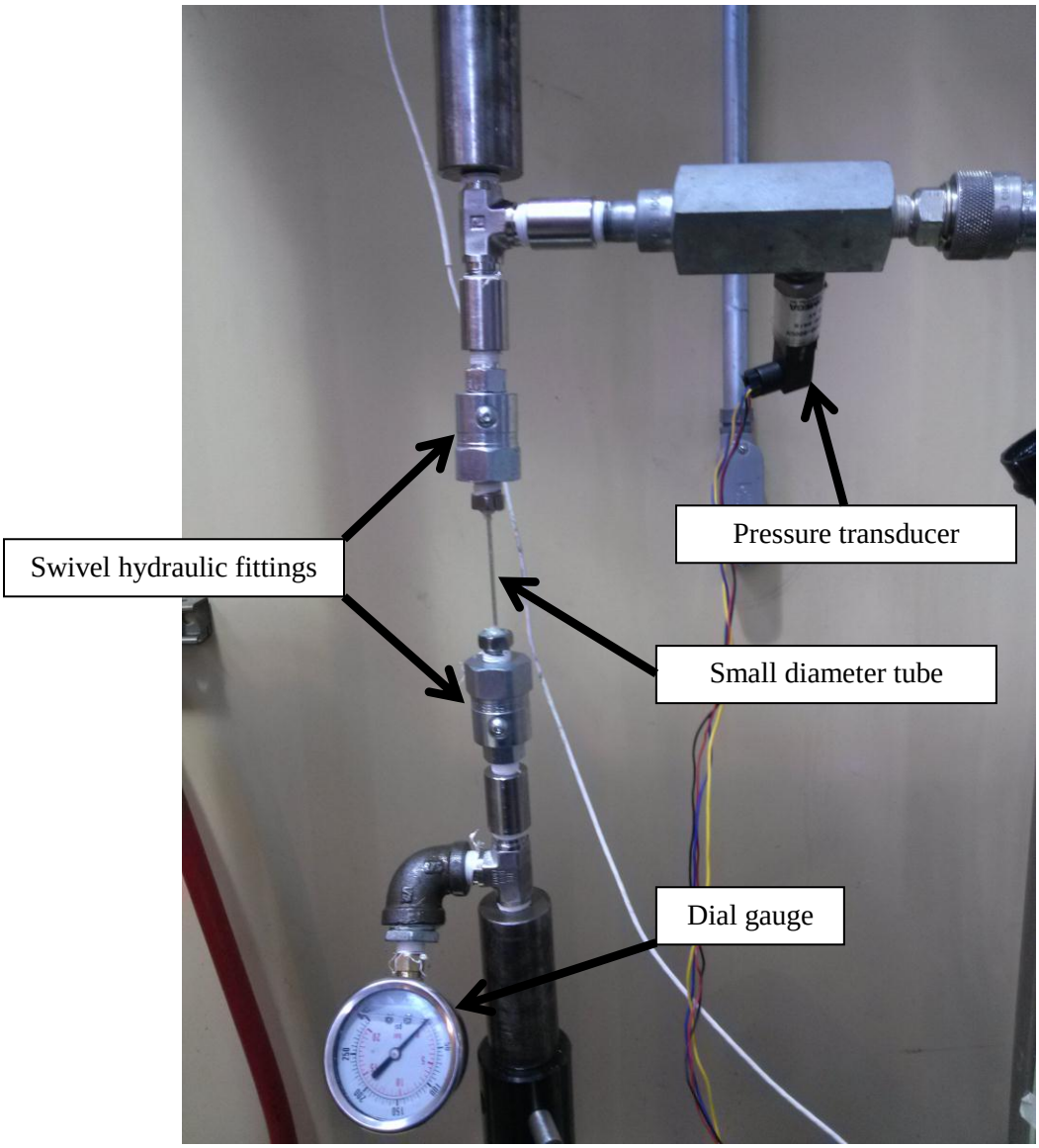

Figure **4-12**: Close-up photograph of the blocked force and axial modulus test setups for braided tubes.

Results

Free Strain

Predictions of performance of the braided F[2]MC tubes were done by Mr. Bin Zhu using both the upper and lower bounds for polyurethane modulus. The elasticity solutions for infinitely long tubes are denoted by "analytic" in the results.

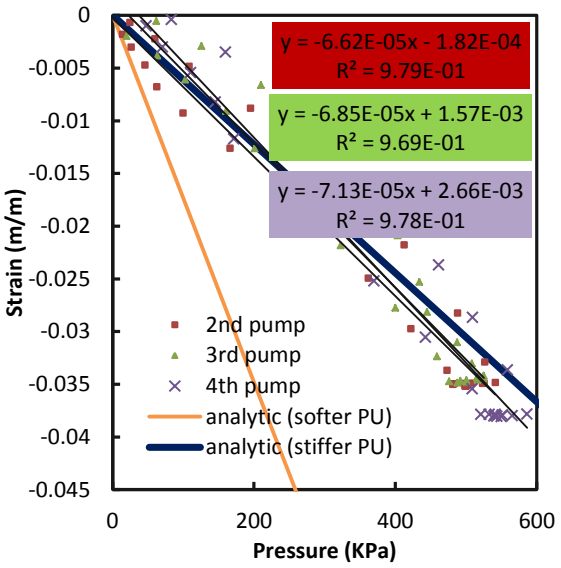

Figure **4-13**: Small braided tubes 24° free strain test A-1.

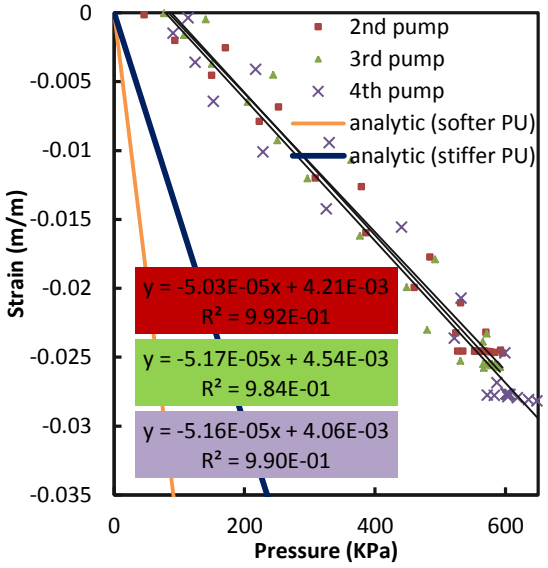

Figure **4-14**: small braided tubes 40° free strain test A-4.

Figures **4-13** and **4-14** show free strain test results for the 24° and 40° tubes, respectively. Graphs for the other free strain tests can be found in Appendix B. In the 24° tube, the experimental and stiffer polyurethane predictions match well, including a small amount of hysteresis in the experimental results. The 40° tube underperforms greatly relative to either type of polyurethane. For both angles, the slope is consistent for consecutive pressurization cycles. These observations are also true for the other free strain tests found in Appendix B conducted for different length tubes (lengths B and C). They both also appear to be very linear over the pressurization/depressurization cycle, as expected.

Blocked Force

Figures **4-15** and **4-16** show results from a blocked force test of each reinforcement angle. The remainder of the graphical results are provided in Appendix B. The 24° tube has a much larger amount of hysteresis than in free strain tests and also less force per unit pressure than predicted. The 40° tube has less hysteresis and a better match to the closely matched predictions. Again, these two examples are similar to all the tests conducted for all other lengths (B and C). It is observed that blocked force is less sensitive to differences in polyurethane stiffness. The results also appear to be very repeatable over subsequent pressurization/depressurization cycles.

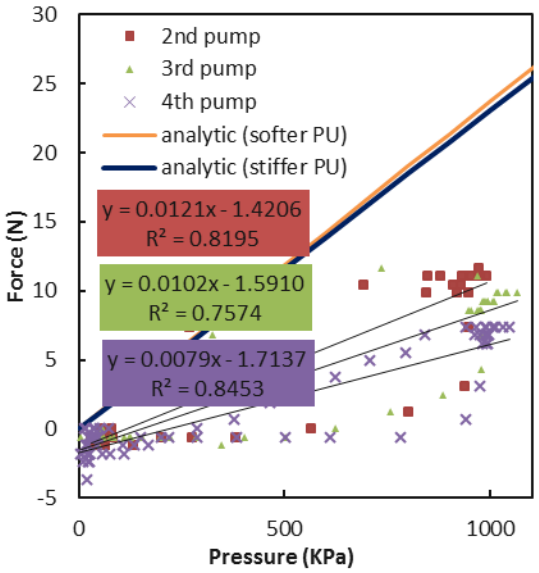

Figure **4-15**: Small braided tubes 24° blocked force test A-1.

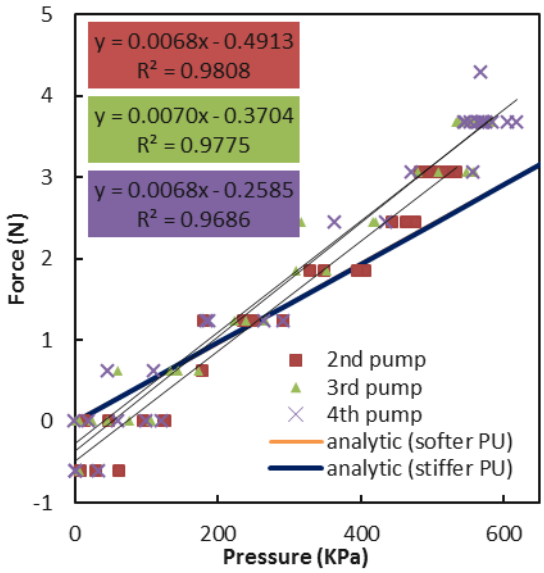

Figure **4-16**: Small braided tubes 40° blocked force test A-1.

Axial Modulus

Figures **4-17** and **4-18** show axial modulus test results for both braid angles. Again, the remainder of the results are located in Appendix B. The 24° tube matches well with the stiffer polyurethane prediction. The 40° tube is much stiffer than predicted with either polyurethane modulus. The trends in these graphs are representative of the other tests with specimens of different lengths. Both tubes behave linearly for at least the 0-2% strain range.

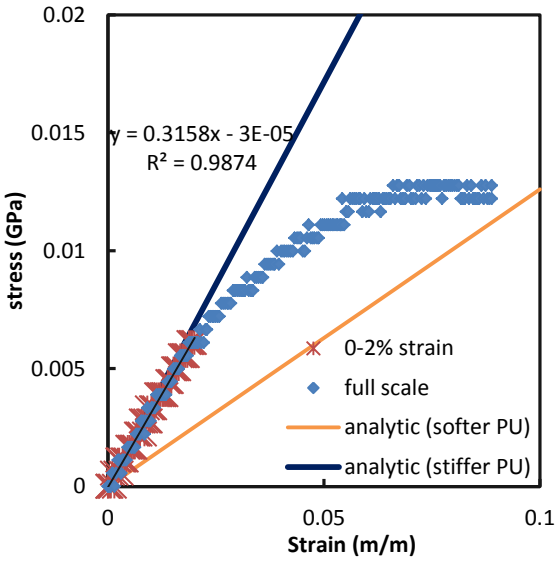

Figure **4-17**: small braided tubes 24° axial modulus test A-3.

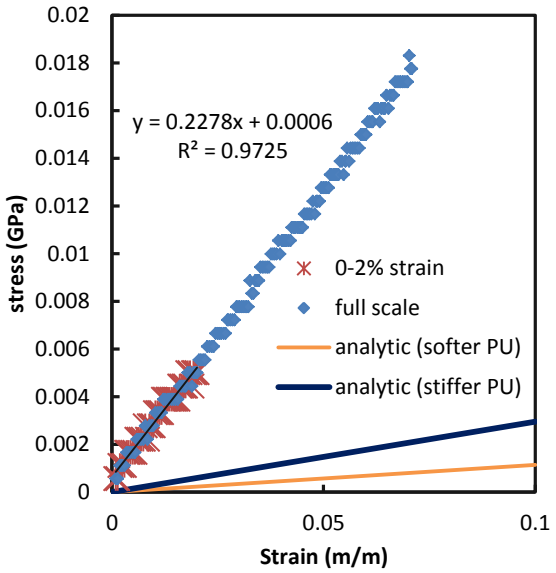

Figure **4-18**: small braided tubes 40° axial modulus test A-1.

Quantitative results

Tables **4-4** to **4-6** contain the quantitative performance results for all the tests conducted with braided tubes. For each individual tube, the slope from graphs such as those shown above was calculated by averaging the second, third, and forth pressure cycles. Cells containing "N/A"

represent tubes that had failed before or during testing such that quantitative results could not be obtained. An average slope based on repeated cycles was computed for each specimen. An average slope from several specimens of similar gage length was then computed. The percent difference between this experimental result and the theoretical result was calculated using equation 4-2 for both the softer and stiffer polyurethane moduli.

$$\%Difference = \left(\frac{experimental - theoretical}{theoretical}\right) \times 100 \quad (4\text{-}2)$$

For all the tests conducted with braided tubes, the experimental results either matched with or were much closer to the predictions made using the stiffer polyurethane modulus. For the following discussions, predictions for the stiffer polyurethane moduli are referenced.

Table **4-4**: Quantitative results for free strain tests of braided tubes.

	56-mm gauge length, Group A		**96-mm gauge length, Group B**		**85-mm gauge length, Group C**	
tube	24° tube FS slopes (1/KPa)	40° tube FS slopes (1/KPa)	24° tube FS slopes (1/KPa)	40° tube FS slopes (1/KPa)	24° tube FS slopes (1/KPa)	40° tube FS slopes (1/KPa)
1	-6.87E-05	-5.48E-05	-4.85E-05	-4.61E-05	-5.60E-05	-5.50E-05
2	N/A	-5.34E-05	-4.45E-05	-5.10E-05	N/A	-4.50E-05
3	-6.74E-05	-5.19E-05	No specimens made			
4	-5.22E-05	-5.12E-05				
Averaged experimental	-6.28E-05	-5.28E-05	-4.65E-05	-4.86E-05	-5.60E-05	-5.00E-05
Theory (softer PU)	-0.00017	-0.00039	-0.00017	-0.00039	-0.00017	-0.00039
% difference (softer PU)	-63	-86	-73	-88	-67	-87
Theory (stiffer PU)	-0.000061	-0.00015	-0.000061	-0.00015	-0.000061	-0.00015
% difference (stiffer PU)	2.9	-65	-24	-68	-8.2	-67

When comparing the predicted and measured free strain slopes in Table **4-3**, it is seen that the 24° tube matches well with the largest difference being about 24% and smallest being

about 3%. On the other hand the 40° tube has much larger difference (about 65%) all around. This repeatability is a good sign that the tests all went well and also that no significant end effects are present between different lengths. However is clear that the 40° tubes are not preforming as predicted for reasons other than experimentation.

Results for the blocked force experiments can be seen in Table **4-5**. These results are a little more scattered as they tend to be for many different types of F^2MC actuators. The 96-mm tube results were discarded due to a bad load cell calibration. The 24° tube of 56 mm length has roughly 58% difference and the 85-mm one closer to 20%. On the other hand, the 56-mm 40° tube is at about 17% and the 85-mm tube is at 44%. This would make it appear that the differences are not related to the length but rather another form of inconsistency in the experiments or tubes.

Table **4-5**: Quantitative results for blocked force tests of braided tubes.

	56-mm gauge length, Group A		**96-mm gauge length, Group B**		**85-mm gauge length, Group C**	
tube	24° tube BF slopes (N/KPa)	40° tube BF slopes (N/KPa)	24° tube BF slopes (N/KPa)	40° tube BF slopes (N/KPa)	24° tube BF slopes (N/KPa)	40° tube BF slopes (N/KPa)
1	0.01	0.00686	Results discarded		0.0183	0.00806
2	N/A	0.00476			N/A	0.0058
3	0.00783	0.00493			No specimens made	
4	0.0115	5.93E-03				
Averaged experimental	0.00978	0.00562			0.01830	0.00693
Theory (softer PU)	0.0237	0.00486			0.0237	0.00486
% difference (softer PU)	-59	16			-23	43
Theory (stiffer PU)	0.023	0.0048			0.023	0.0048
% difference (stiffer PU)	-57	17			-20	44

Table **4-6** contains the axial modulus results. The longest length tube data were discarded due to a bad load cell calibration. For these experiments, the 24° tube matches predictions well with differences at 33% and 14%, but the 40° tube is far stiffer than predicted with differences of about 260% and 760%.

Table **4-6**: Quantitative results for axial modulus tests of braided tubes.

	56-mm gauge length, Group A		**96-mm gauge length, Group B**		**85-mm gauge length, Group C**	
tube	24° tube axial modulus (GPa)	40° tube axial modulus (GPa)	24° tube axial modulus (GPa)	40° tube axial modulus (GPa)	24° tube axial modulus (GPa)	40° tube axial modulus (GPa)
1	N/A	0.227	Results discarded		0.398	0.119
2	N/A	0.267			0.386	0.096
3	0.315	0.251			No specimens made	
4	0.598	0.291				
Averaged experimental	0.456	0.259			0.392	0.107
Theory (softer PU)	0.126	0.011			0.126	0.0114
% difference (softer PU)	260	2200			210	840
Theory (stiffer PU)	0.344	0.03			0.344	0.03
% difference (stiffer PU)	33	770			13.95	260

Conclusions and recommendations

It was shown that it is possible to produce and use tubes as F^2MC actuators of a much smaller diameter then previously tested. Although there was some amount of underperformance

in some cases, they were shown deform as predicted under pressurization and that they could serve useful in future tests in adaptive structures where larger tubes would be overly bulky.

Additional experiments are recommended to generalize these results for other fiber angles in the F^2MC actuators and other stiffnesses of surrounding media. It is also recommended that attempts to increase the fiber coverage or volume fraction to allow for greater pressures for testing. Detailed evaluation of the three-dimensional constitutive behavior of the FMC material is recommended as well.

References

1. Philen,M., Shan, Y., Bakis, C. E., Wang, K. W, and Rahn, C. D., "Variable Stiffness Adaptive Structures Utilizing Hydraulically Pressurized Flexible Matrix Composites with Valve Control," *14th AIAA/ASME/AHS Adaptive Structures Conference*, AIAA-2006-2134, Newport, RI, May 2006.

2. Philen, M., Shan, Y., Prakash, P., Wang, K., Rahn, C., Zydney, A., Bakis, C., "Fibrillar Network Adaptive Structure with Ion Transport Actuation," Journal of Intelligent Material Systems and Structures 18 (2007): 323-34.

3. Y. Shan, and C.E. Bakis, "Flexible Matrix Actuators," *Proc. 29th Annual Technical Conference, American Society for Composites*, Philadelphia, PA (2005).

4. Y. Shan, C.E. Bakis, M. Philen, K.W. Wang, and C.D. Rahn, "Nonlinear Finite Axisymmetric Deformation of Flexible Matrix Composite Membranes under Internal Pressurization and Axial Force," *Compos. Sci. Technol*. 66 (2006): 3053-3066.

5. Moorhouse, D., Sanders, B., Von Spakovsky, M., and Butt, J., "Benefits and Design Challenges of Adaptive Structures for Morphing Aircraft," *Aeronautical J.* 110 (2006): 157-62.

6. Rufino, R.J., Miller, T.F., and Gandhi, F.S., "Morphing Hull Concepts for Unmanned Underwater Vehicles," *Proc. OCEANS 2008,* Quebec City, QC, 15-18 Sept. 2008, IEEE, CD ROM, 11 p.

7. Daynes, S., and Weaver, P.M., "A Shape Adaptive Airfoil for a Wind Turbine Blade." *Proc. SPIE 7979* (2011): 7979H-1, 11 p.

8. Del Grosso, A.E., and Basso, P., "Adaptive Building Skin Structures." *Smart Materials and Structures* 19 (2010): 124011, 12 p.

9. Zhu, B., Rahn, C.D., and Bakis, C.E., "Actuation of Fluidic Flexible Matrix Composites in Structural Media," *J. Intelligent Material Systems and Structures* 23 (2012): 269-78.

10. HexTow AS4D Product Data Sheet, Hexcel Corp., Stamford, CT, Mar. 2010.

11. "ReoFlex Series Liquid Urethane Rubbers." http://www.smooth-on.com/tb/files/REOFLEX_SERIES.pdf. Smooth-On, Inc., Easton, PA, 5 Jan. 2012.

12. Mullins, L., Tobin, N.R., Harwood, J.A.C., and Payne, A.R., "Stress Softening in Rubber Vulcanizates—3." *J. Applied Polymer Science* 10 (1966): 315-24.

13. Philen, M., Shan, U., Wang, K., Bakis, C., and Rahn, C., "Fluidic Flexible Matrix Composites for the Tailoring of Variable Stiffness Adaptive Structures," *48th AIAA/ASME/ASCE/AHS/ASC Structures, Structural Dynamics, and Materials Conference*, AIAA-2007-1703, Honolulu, HI, April 2007.

Appendix A: New England Wire Documents

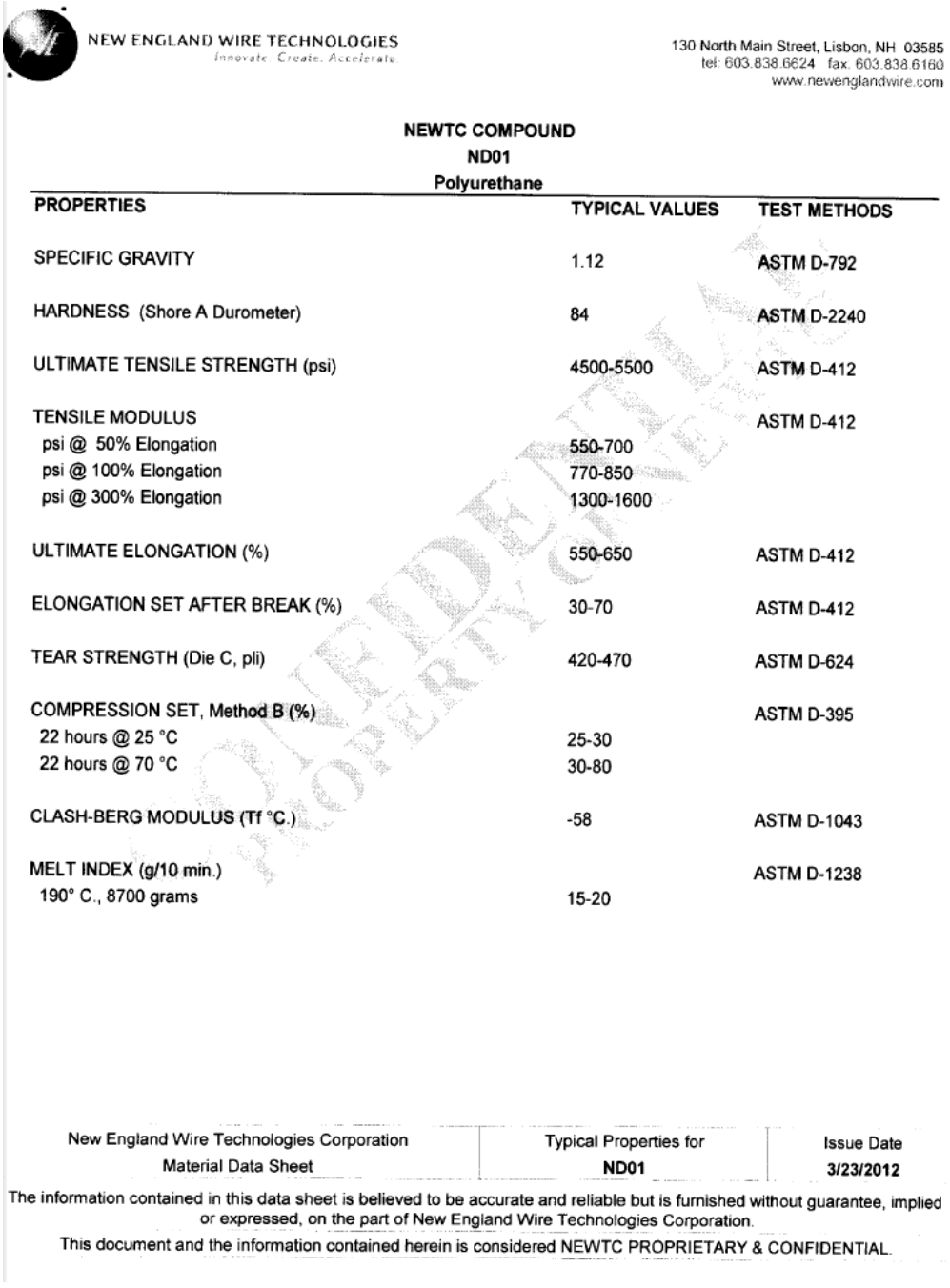

NEW ENGLAND WIRE TECHNOLOGIES
Innovate. Create. Accelerate.

130 North Main Street, Lisbon, NH 03585
tel: 603.838.6624 fax: 603.838.6160
www.newenglandwire.com

NEWTC COMPOUND
ND01
Polyurethane

PROPERTIES	TYPICAL VALUES	TEST METHODS
SPECIFIC GRAVITY	1.12	ASTM D-792
HARDNESS (Shore A Durometer)	84	ASTM D-2240
ULTIMATE TENSILE STRENGTH (psi)	4500-5500	ASTM D-412
TENSILE MODULUS		ASTM D-412
psi @ 50% Elongation	550-700	
psi @ 100% Elongation	770-850	
psi @ 300% Elongation	1300-1600	
ULTIMATE ELONGATION (%)	550-650	ASTM D-412
ELONGATION SET AFTER BREAK (%)	30-70	ASTM D-412
TEAR STRENGTH (Die C, pli)	420-470	ASTM D-624
COMPRESSION SET, Method B (%)		ASTM D-395
22 hours @ 25 °C	25-30	
22 hours @ 70 °C	30-80	
CLASH-BERG MODULUS (Tf °C.)	-58	ASTM D-1043
MELT INDEX (g/10 min.)		ASTM D-1238
190° C., 8700 grams	15-20	

Figure **A-1**: NEW polyurethane data sheet.

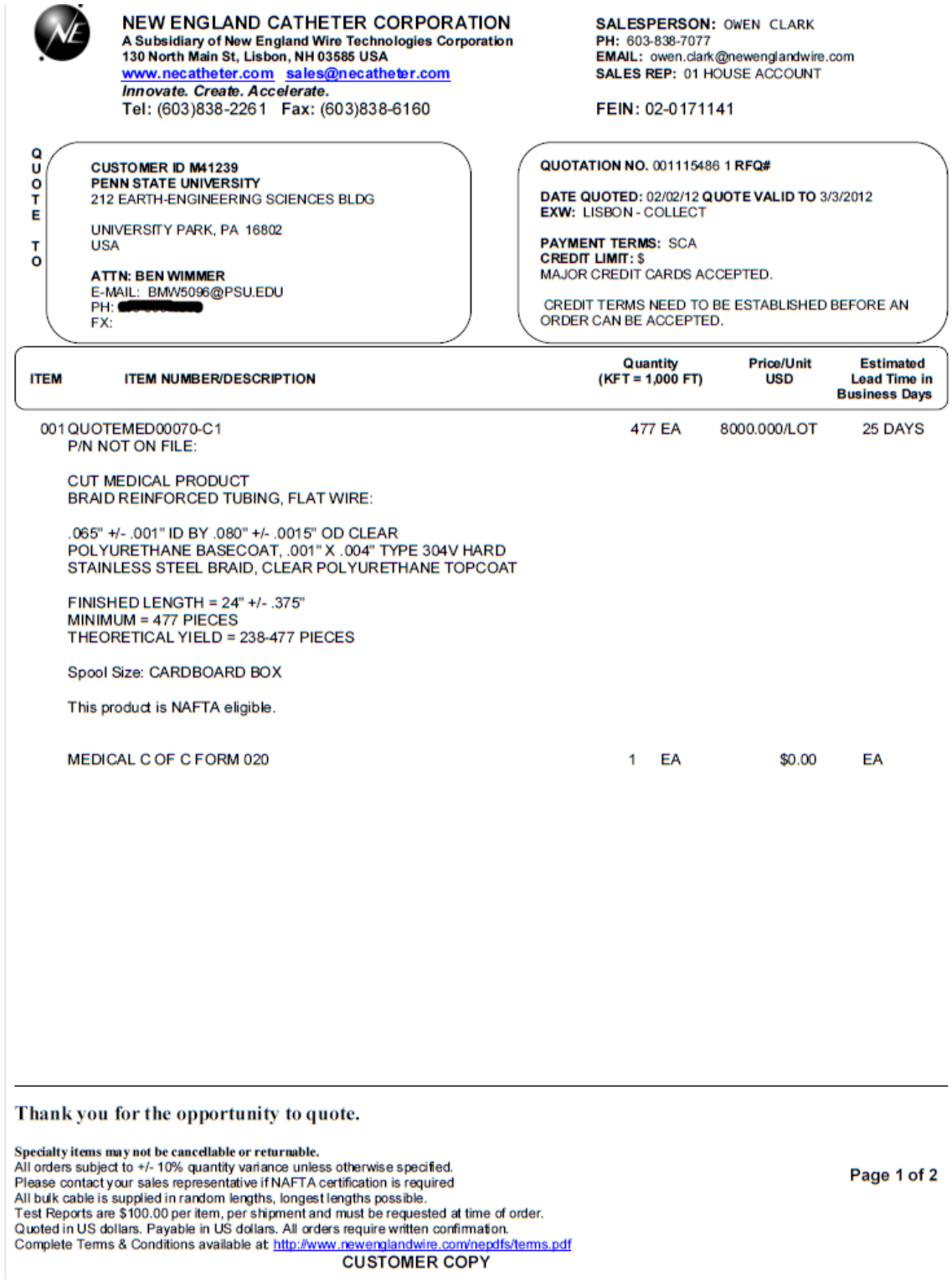

NEW ENGLAND CATHETER CORPORATION
A Subsidiary of New England Wire Technologies Corporation
130 North Main St, Lisbon, NH 03585 USA
www.necatheter.com sales@necatheter.com
Innovate. Create. Accelerate.
Tel: (603)838-2261 Fax: (603)838-6160

SALESPERSON: OWEN CLARK
PH: 603-838-7077
EMAIL: owen.clark@newenglandwire.com
SALES REP: 01 HOUSE ACCOUNT

FEIN: 02-0171141

QUOTE TO

CUSTOMER ID M41239
PENN STATE UNIVERSITY
212 EARTH-ENGINEERING SCIENCES BLDG

UNIVERSITY PARK, PA 16802
USA

ATTN: BEN WIMMER
E-MAIL: BMW5096@PSU.EDU
PH: [redacted]
FX:

QUOTATION NO. 001115486 1 **RFQ#**

DATE QUOTED: 02/02/12 **QUOTE VALID TO** 3/3/2012
EXW: LISBON - COLLECT

PAYMENT TERMS: SCA
CREDIT LIMIT: $
MAJOR CREDIT CARDS ACCEPTED.

CREDIT TERMS NEED TO BE ESTABLISHED BEFORE AN ORDER CAN BE ACCEPTED.

ITEM	ITEM NUMBER/DESCRIPTION	Quantity (KFT = 1,000 FT)	Price/Unit USD	Estimated Lead Time in Business Days
001	QUOTEMED00070-C1 P/N NOT ON FILE: CUT MEDICAL PRODUCT BRAID REINFORCED TUBING, FLAT WIRE: .065" +/- .001" ID BY .080" +/- .0015" OD CLEAR POLYURETHANE BASECOAT, .001" X .004" TYPE 304V HARD STAINLESS STEEL BRAID, CLEAR POLYURETHANE TOPCOAT FINISHED LENGTH = 24" +/- .375" MINIMUM = 477 PIECES THEORETICAL YIELD = 238-477 PIECES Spool Size: CARDBOARD BOX This product is NAFTA eligible.	477 EA	8000.000/LOT	25 DAYS
	MEDICAL C OF C FORM 020	1 EA	$0.00	EA

Thank you for the opportunity to quote.

Specialty items may not be cancellable or returnable.
All orders subject to +/- 10% quantity variance unless otherwise specified.
Please contact your sales representative if NAFTA certification is required
All bulk cable is supplied in random lengths, longest lengths possible.
Test Reports are $100.00 per item, per shipment and must be requested at time of order.
Quoted in US dollars. Payable in US dollars. All orders require written confirmation.
Complete Terms & Conditions available at: http://www.newenglandwire.com/nepdfs/terms.pdf

Page 1 of 2

CUSTOMER COPY

Figure **A-2**: NEW quote page 1 of 2.

NEW ENGLAND CATHETER CORPORATION
A Subsidiary of New England Wire Technologies Corporation
130 North Main St, Lisbon, NH 03585 USA
www.necatheter.com sales@necatheter.com
Innovate. Create. Accelerate.
Tel: (603)838-2261 Fax: (603)838-6160

SALESPERSON: OWEN CLARK
PH: 603-838-7077
EMAIL: owen.clark@newenglandwire.com
SALES REP: 01 HOUSE ACCOUNT

FEIN: 02-0171141

QUOTE TO

CUSTOMER ID M41239
PENN STATE UNIVERSITY
212 EARTH-ENGINEERING SCIENCES BLDG

UNIVERSITY PARK, PA 16802
USA

ATTN: BEN WIMMER
E-MAIL: BMW5096@PSU.EDU
PH: [redacted]
FX:

QUOTATION NO. 001115486 1 **RFQ#**

DATE QUOTED: 02/02/12 **QUOTE VALID TO** 3/3/2012
EXW: LISBON - COLLECT

PAYMENT TERMS: SCA
CREDIT LIMIT: $
MAJOR CREDIT CARDS ACCEPTED.

CREDIT TERMS NEED TO BE ESTABLISHED BEFORE AN ORDER CAN BE ACCEPTED.

ITEM	ITEM NUMBER/DESCRIPTION	Quantity (KFT = 1,000 FT)	Price/Unit USD	Estimated Lead Time in Business Days
002	QUOTEMED00073-C1 P/N NOT ON FILE: CUT MEDICAL PRODUCT BRAID REINFORCED TUBING, FLAT WIRE: .065" +/- .001" ID BY .080" +/- .0015" OD CLEAR POLYURETHANE BASECOAT, .001" X .006" TYPE 304V HARD STAINLESS STEEL BRAID, OVER 1/UNDER 1, CLEAR POLYURETHANE TOPCOAT FINISHED LENGTH = 24" +/- .375" MINIMUM = 500 PIECES THEORETICAL YIELD = 250-500 PIECES Spool Size: CARDBOARD BOX This product is NAFTA eligible.	500 EA	6495.000/LOT	25 DAYS
	MEDICAL C OF C FORM 020	1 EA	$0.00	EA

CREDIT TERMS NEED TO BE ESTABLISHED BEFORE AN ORDER CAN BE ACCEPTED. PLEASE CONTACT CHRISTINA IANNO IN ACCOUNTS RECEIVABLE AT christina.ianno@newenglandwire.com

PLEASE CONTACT YOUR NEWTC SALESPERSON IF YOU ARE INTERESTED IN PLACING AN ORDER USING A CREDIT CARD.

Thank you for the opportunity to quote.

Specialty items may not be cancellable or returnable.
All orders subject to +/- 10% quantity variance unless otherwise specified.
Please contact your sales representative if NAFTA certification is required
All bulk cable is supplied in random lengths, longest lengths possible.
Test Reports are $100.00 per item, per shipment and must be requested at time of order.
Quoted in US dollars. Payable in US dollars. All orders require written confirmation.
Complete Terms & Conditions available at: http://www.newenglandwire.com/nepdfs/terms.pdf

Page 2 of 2

CUSTOMER COPY

Figure **A-3**: NEW quote page 2 of 2.

Appendix B: Additional Graphs for Braided Tubes

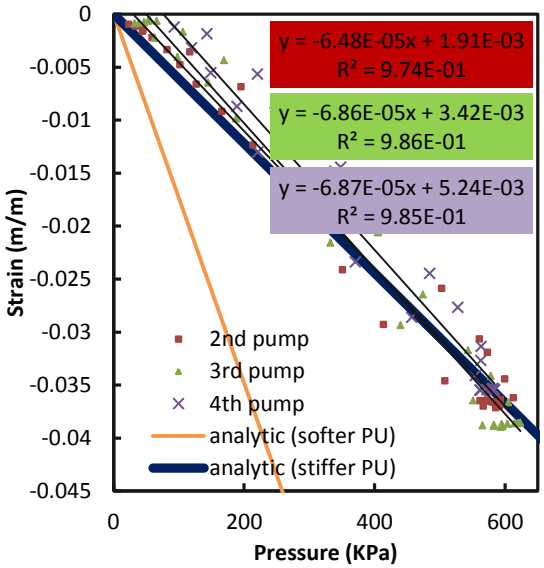

Figure **B-1**: Small braided tubes 24° Free strain test A-3.

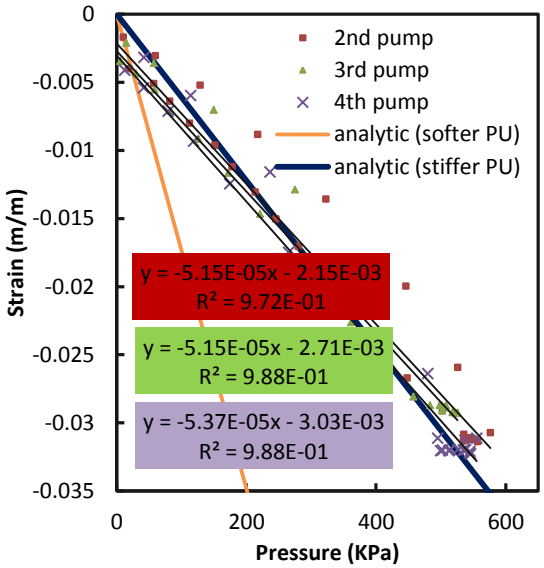

Figure **B-2**: Small braided tubes 24° Free strain test A-4.

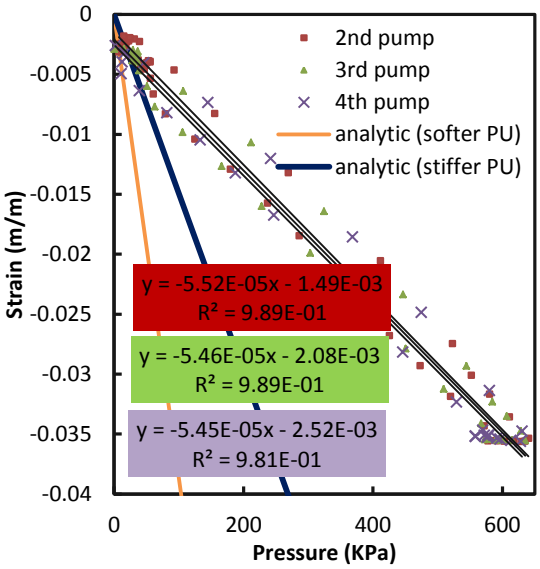

Figure **B-3**: Small braided tubes 40° free strain test A-1.

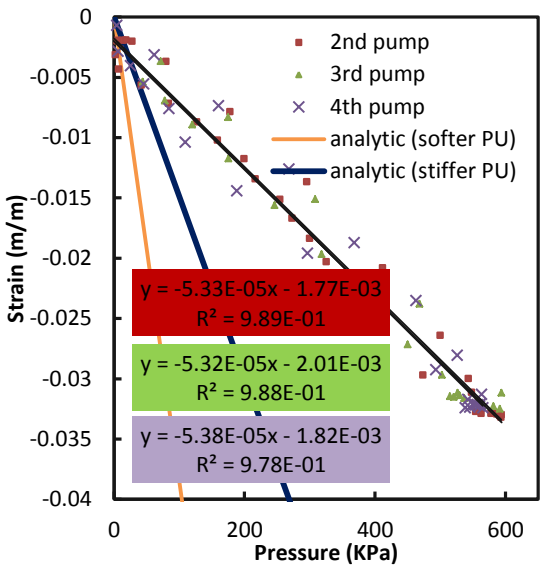

Figure **B-4**: Small braided tubes 40° free strain test A-2.

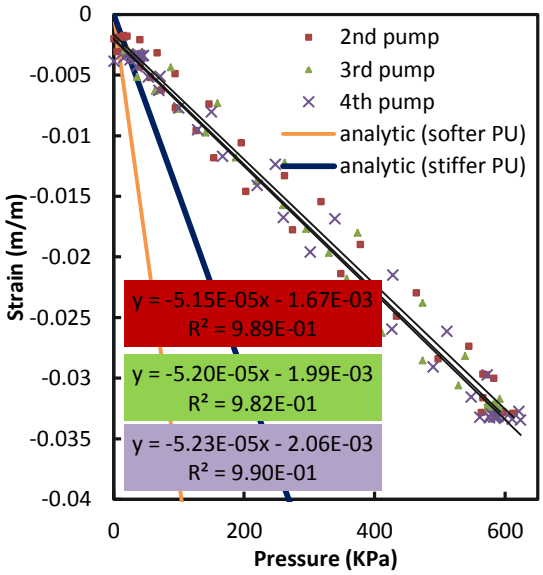

Figure **B-5**: Small braided tubes 40° free strain test A-3.

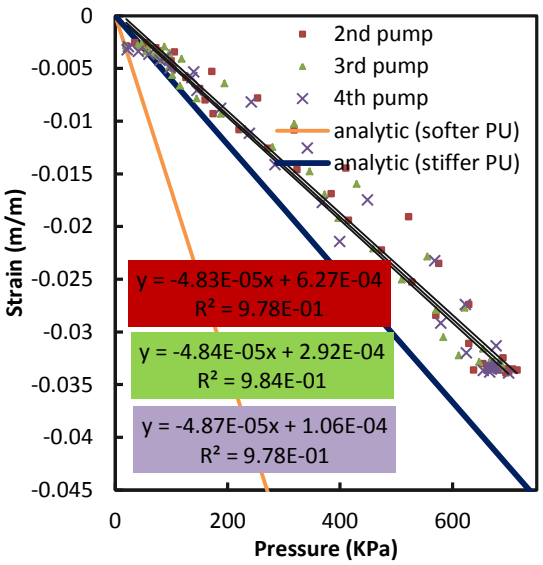

Figure **B-6**: Small braided tubes 24° free strain test B-1.

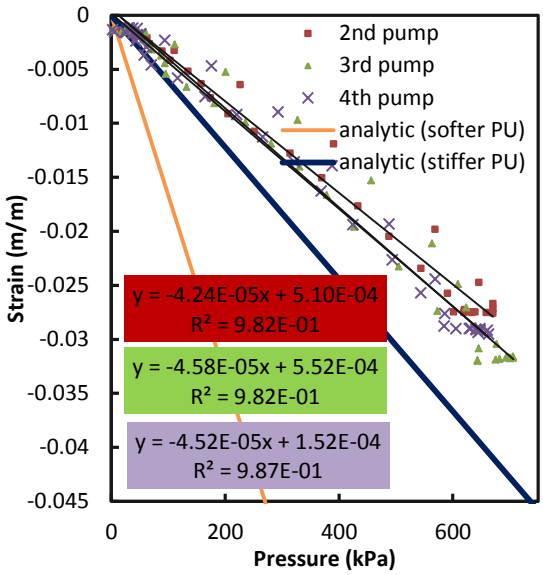

Figure **B-7**: Small braided tubes 24° free strain test B-2.

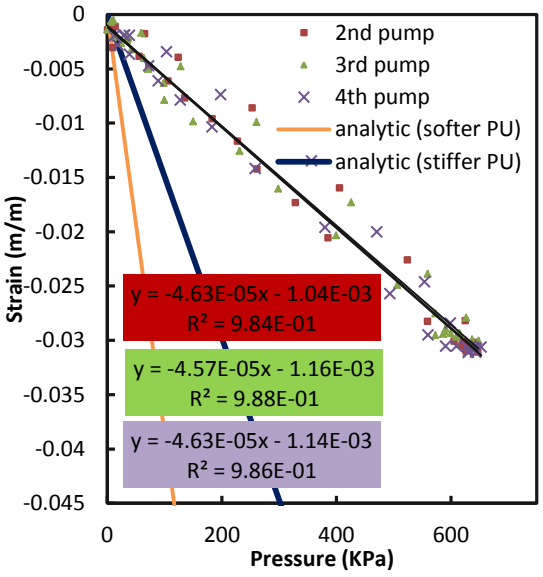

Figure **B-8**: Small braided tubes 40°free strain test B-1.

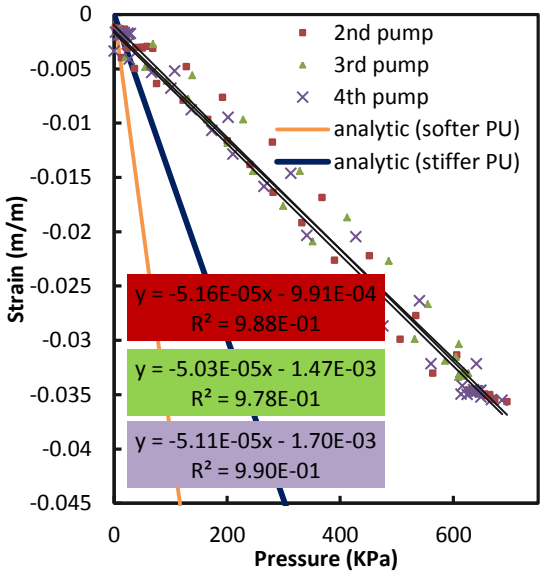

Figure **B-9**: Small braided tubes 40° free strain test B-2.

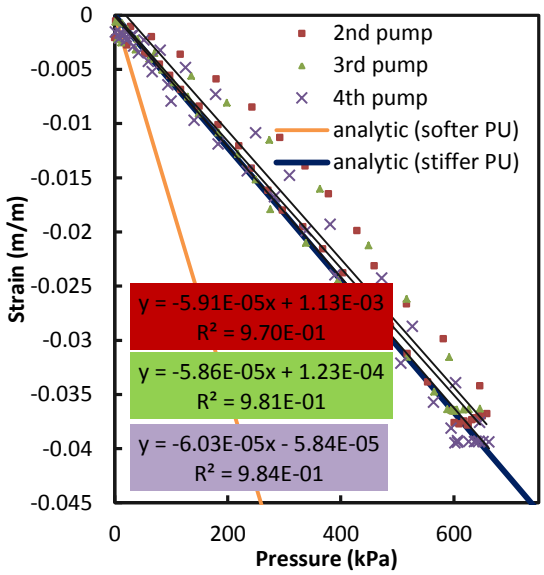

Figure **B-10**: Small braided tubes 24° free strain test B-1.

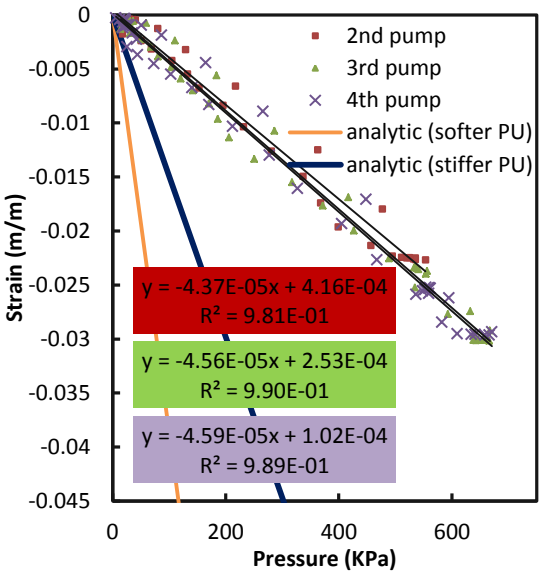

Figure **B-11**: Small braided tubes 40° free strain test C-1.

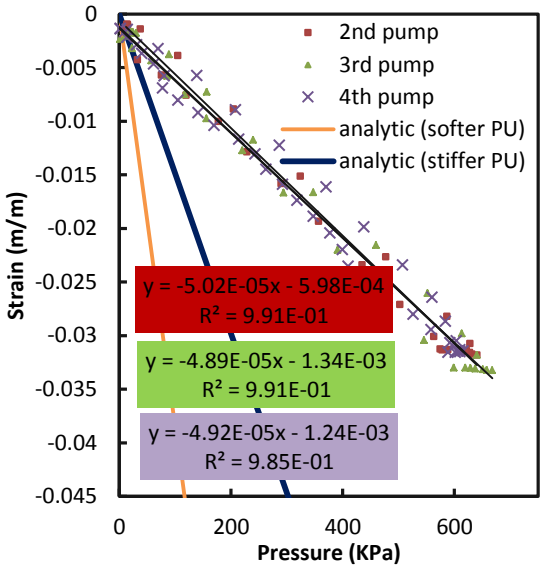

Figure **B-12**: Small braided tubes 40° free strain test C-2.

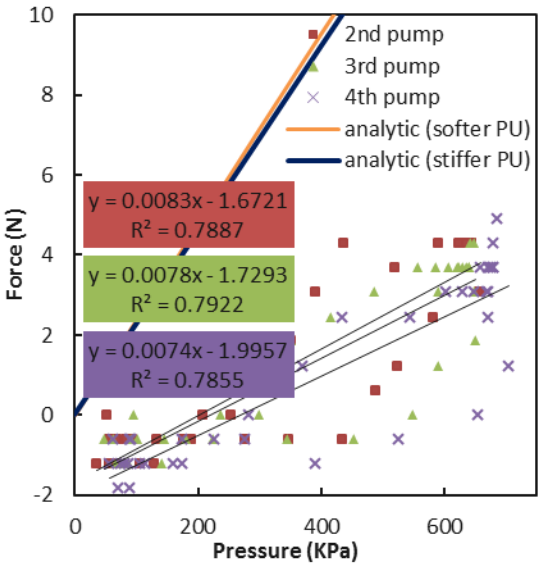

Figure **B-13**: Small braided tubes 24° blocked force test A-3.

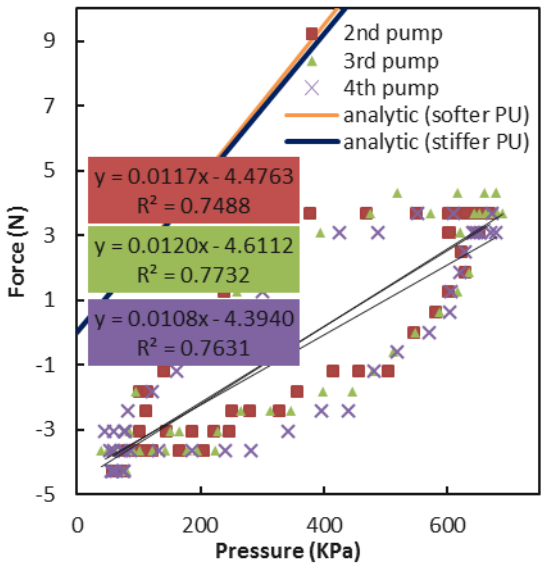

Figure **B-14**: Small braided tubes 24° blocked force test A-4.

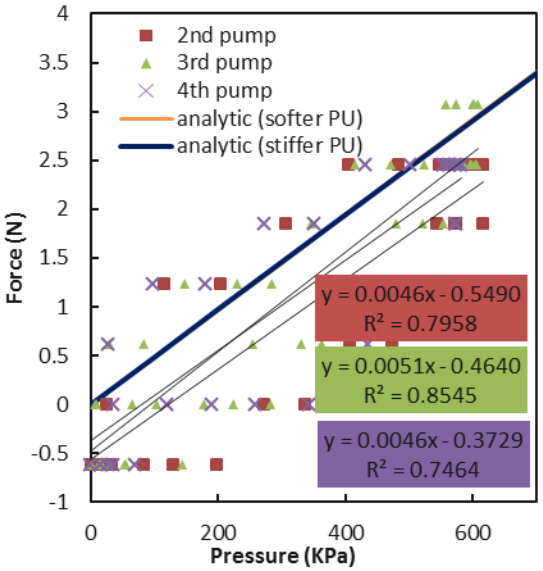

Figure **B-15**: small braided tubes 40° blocked force test A-2.

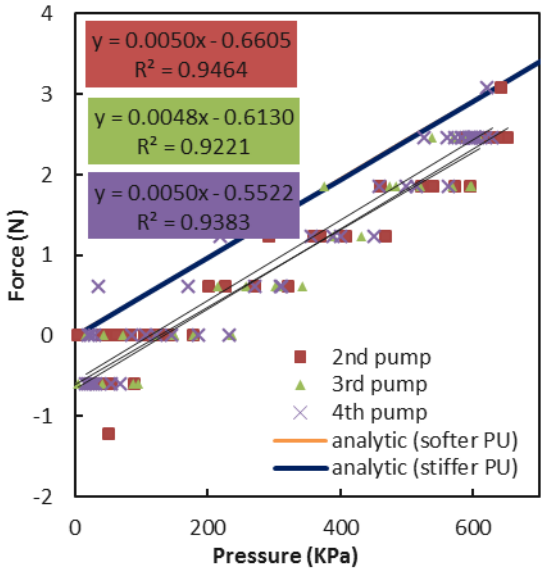

Figure **B-16**: small braided tubes 40° blocked force test A-3.

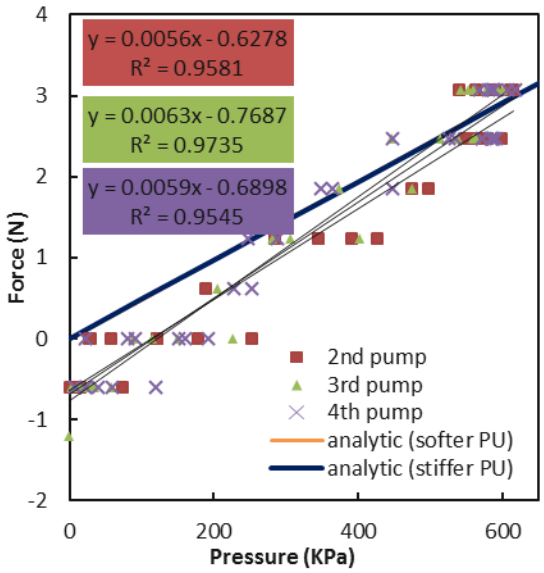

Figure **B-17**: small braided tubes 40° blocked force test A-4.

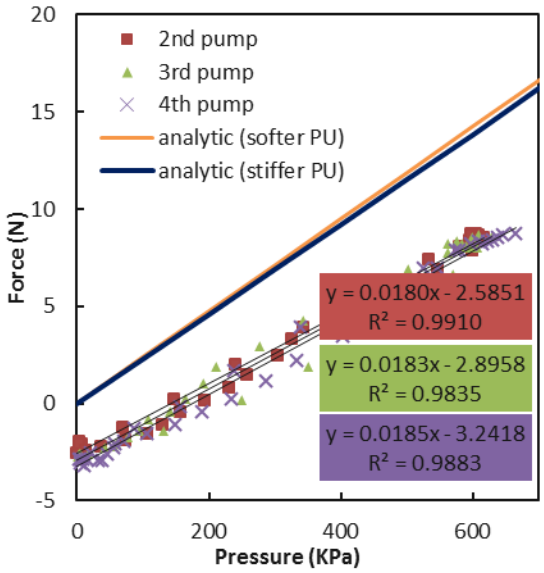

Figure **B-18**: Small braided tubes 24° blocked force test C-1.

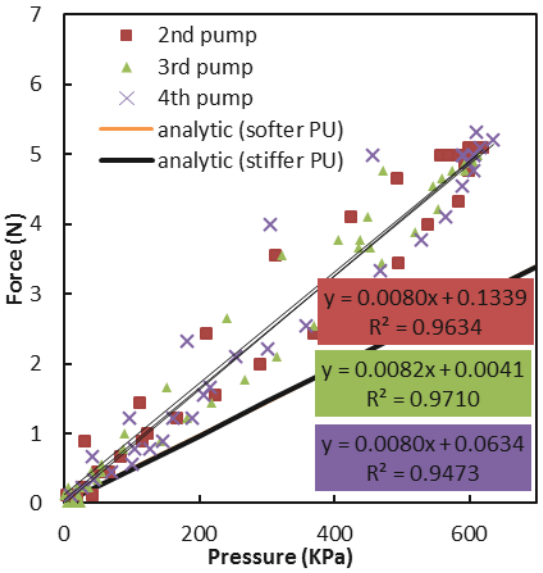

Figure **B-19**: Small braided tubes 40° blocked force test C-1.

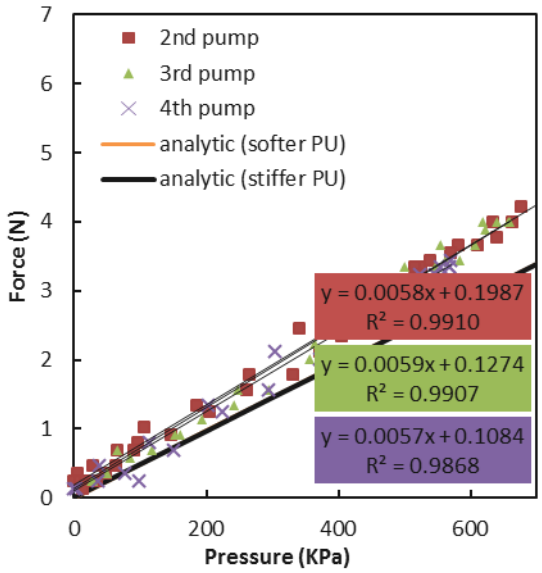

Figure **B-20**: Small braided tubes 40° blocked force test C-2.

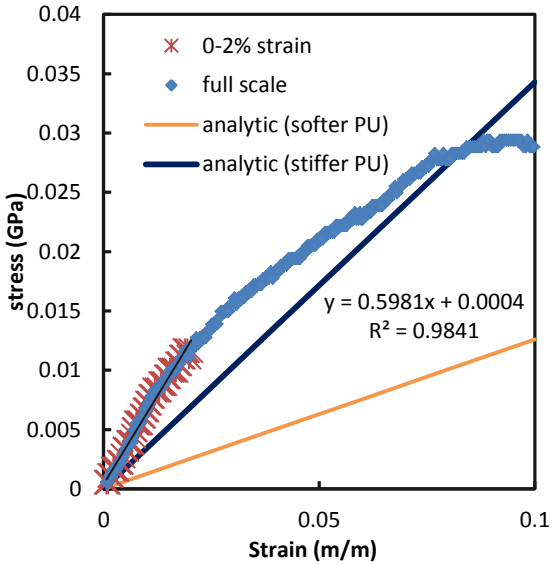

Figure **B-21**: Small braided tubes 24° axial modulus test A-4.

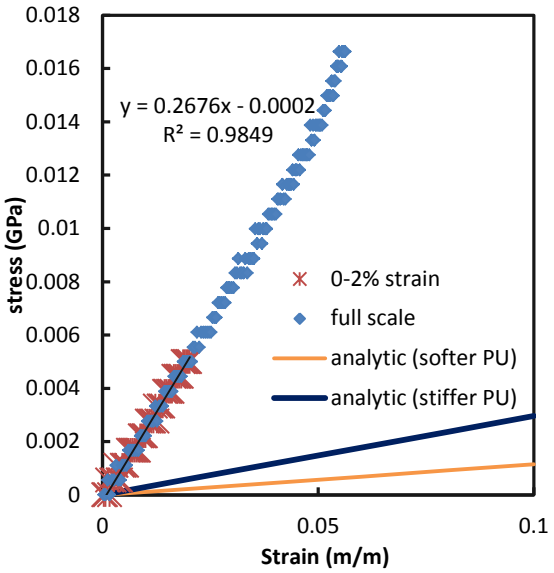

Figure **B-22**: Small braided tubes 40° axial modulus test A-2.

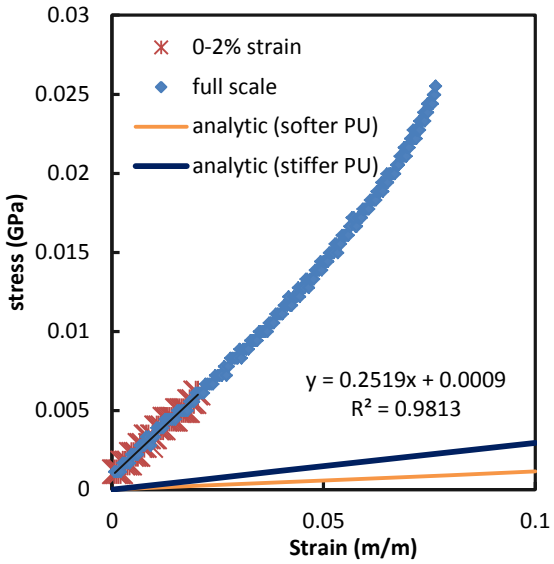

Figure **B-23**: Small braided tubes 40° axial modulus test A-3.

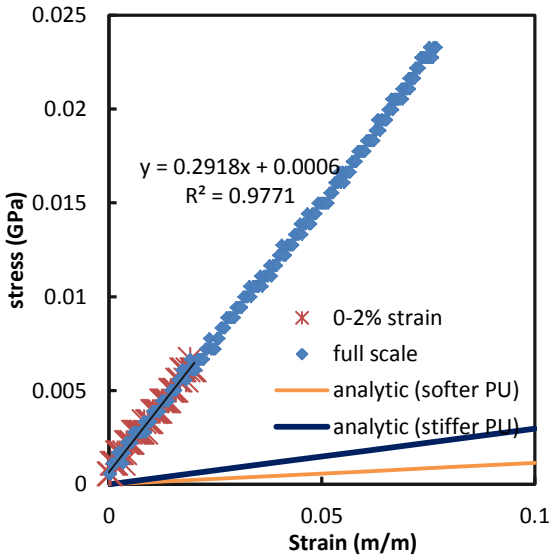

Figure **B-24**: Small braided tubes 40° axial modulus test A-4.

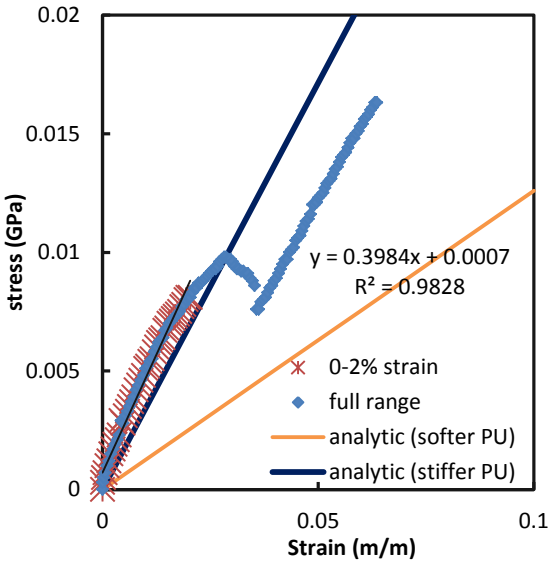

Figure **B-25**: Small braided tubes 24° axial modulus test C-1.

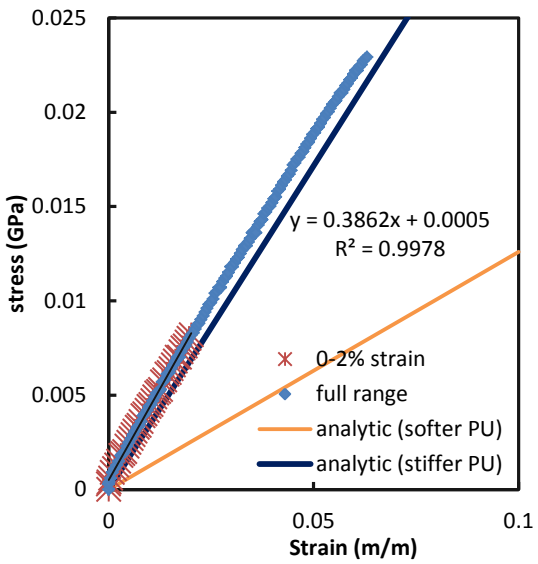

Figure **B-26**: Small braided tubes 24° axial modulus test C-2.

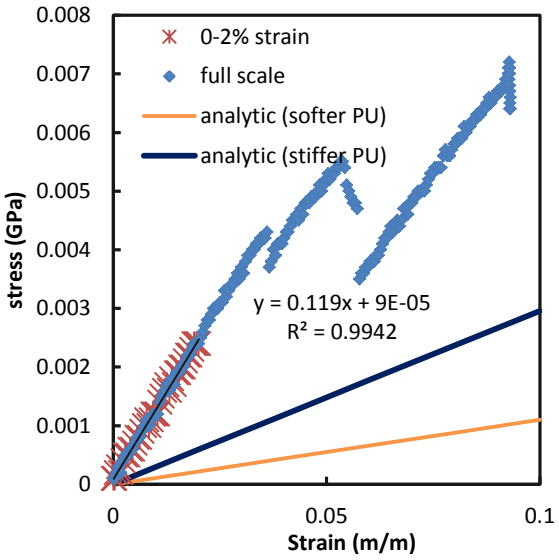

Figure **B-27**: Small braided tubes 40° axial modulus test C-1.

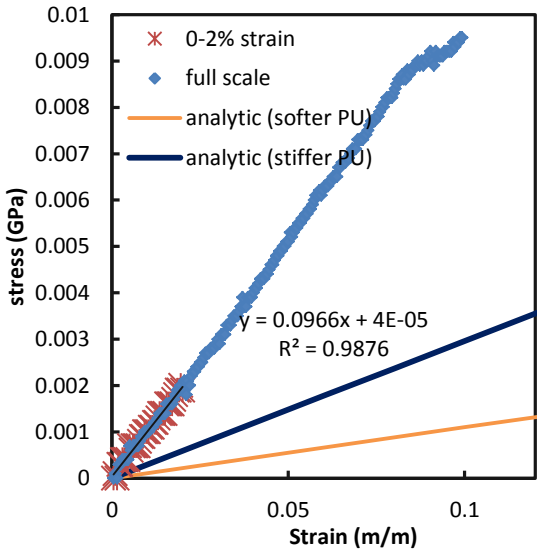

Figure **B-28**: Small braided tubes 40° axial modulus test C-2.